MedCrave
Step into the World of Research

Aeronautics and Aerospace Open Access Journal

Research Article

Open Access

CrossMark

High-performing hydrogen peroxide hybrid rocket with 3-D printed and extruded ABS fuel

Abstract

Development of a high-performing hybrid rocket system that employs 90% hydrogen peroxide and 3-D printable thermoplastic materials is reported. Traditionally, high-grade peroxide has been employed as a monopropellant using noble-metal catalysts to initiate thermal decomposition. Catbeds beds are expensive, heavy, and contribute no propulsive mass to the system. Catbeds exhibit limited operational lifetimes, and are often rendered inactive due to the high temperatures of thermal decomposition. The presented alternative thermally-decomposes the injected peroxide stream using an electrostatic ignition system, where as a moderate electric field is introduced to the additively layered ABS fuel grain. Electrostatic arcs are induced within the 3-D printed surface features, and produce sufficient pyrolyzed fuel vapor to induce spontaneous combustion when a flow of gaseous oxygen is introduced. Heat released is sufficient to thermally decompose the injected peroxide stream. The liberated heat and oxygen from decomposition drive full combustion along the length of the fuel grain. Gaseous oxygen pre-leads as small as 250ms reliably initiate combustion. Multiple on-demand relights are provided with this system. Achieved laboratory specific impulse values exceed 215s under ambient conditions, with a projected vacuum value exceeding 300s. Density specific impulse values exceeding 4000N-s/liter are achievable with this system.

Volume 2 Issue 6 - 2018

Stephen A Whitmore,[1] Isaac W Armstrong,[2] Mark C Heiner,[2] Christopher J Martinez[2]

[1]Professor, Mechanical and Aerospace Engineering Department, Utah State University, USA

[2]Graduate Research Assistant, Mechanical and Aerospace Engineering Department, Utah State University, USA

Correspondence: Stephen A Whitmore, Professor, Mechanical and Aerospace Engineering Department, Utah State University, Logan Utah, 84322-4130, USA, Tel 435-797-2951

Email stephen.whitmare@usu.edu

Received: October 05, 2018 | **Published:** November 20, 2018

Nomenclature

A_c	Fuel port cross-sectional area, cm^2
A_e	Nozzle exit area, cm^2
A_{exit}	Nozzle exit area, cm^2
A^*	Cross-sectional area at nozzle choke, cm^2
a	Scale factor, $(cm/s)-(g/cm^2-sec^j)^{-n}$
C_F	Thrust coefficient
D_{port}	Instantaneous fuel port diameter, cm
D_{0port}	Initial fuel port diameter, cm
f	Peroxide mass concentration
G_{ox}	Oxidizer massflux, g/cm^2-s
G_{tot}	Total massflux, g/cm^2-s
g_0	Acceleration of gravity, $9.8067\ m/sec^2$
I_{sp}	Specific impulse, sec
L_{port}	Fuel grain length, cm
M	Generic Mass, g
M_{fuel}	Fuel mass, g
ΔM_{fuel}	Consumed fuel mass, g
M_w	Molecular weight, $kg/kg\text{-}mol$
$\dot{m}_{fuel}$	Fuel massflow, g/s
$\dot{m}_{GOX}$	Gaseous oxygen oxidizer massflow, g/s
$\dot{m}_{H2O2}$	Hydrogen peroxide oxidizer massflow, g/s
$\dot{m}_{ox}$	Oxidizer massflow, g/s
$\dot{m}_{total}$	Total massflow through nozzle exit, g/s
O/F	Oxidizer/fuel ratio
P_{catbed}	Catbed exit pressure, $psia$
$P_{chamber}$	Pressure at combustor inlet, $psia$
P_0	Chamber stagnation pressure, $psia$
R_g	Gas constant, $J/kg\text{-}K$
$\dot{r}$	Linear regression rate of fuel, cm/s
S_g	Effective specific gravity of propellants
$P_{chamber}$	Temperature at combustor inlet, $psia$
T_0	Stagnation or flame temperature, K
$T_{0actual}$	Actual stagnation (flame) temperature, K
T_{0ideal}	Ideal stagnation (flame) temperature, K
T_{hrust}	Calculated thrust level, N
t	Time, s
t_{final}	Final burn time, s
t_{burn}	total burn time, s
t_0	Time of burn initiation, s
η	Catalyst decomposition efficiency
η^*	Combustion efficiency
ϕ	Equivalence ratio
γ	Ratio of specific heats
ρ_{fuel}	Solid fuel density, g/cm^3
ρ_{H2Ostd}	Standard density of water, $1.0\ g/cm^3$
ρ_{ox}	Oxidizer density, g/cm^3
ρ_{Isp}	Density specific impulse, $N\text{-}s/liter$

Introduction

Although the market for commercially designed and manufactured small spacecraft has grown enormously during the last decade, technology development has mostly centered on spacecraft bus design and miniaturization of sensor components. The space-launch industry has generally not kept pace with the growth trend. With the current state-of-the art, the only available for small commercial, commercial or academic payloads to reach orbit is by "rideshare." A "rideshare" is defined as a secondary payload, smaller in size and weight than the primary payload, that is placed into orbit by a launch vehicle that is mostly paid for by the primary sponsor. Because the sponsor pays the lion's share of the launch costs, the secondary payload receives a substantially reduced launch price in exchange for trade-offs with regard to the payload's final orbit and launch schedule. These tradeoffs typically include having little or no control over the launch date and time, the final orbital parameters, or the ability to halt the launch and remove the payload should a payload failure occur during ground processing prior to launch.

Currently, these "rideshare" services are primarily provided by the DoD/NASA Evolved Expendable Launch Vehicle (EELV) using its secondary payload adapter (ESPA).[1] SpaceX has also offered some secondary payload slots on its Falcon 9 launches; but these opportunities are limited.[2] So unfortunately, with the current state of world launch capability, inadequate low earth orbit (LEO) "rideshare" launch opportunities are available to accommodate the demand for these NanoSat demonstration missions. Furthermore, only a few specialized launch vehicles have upper stages with the ability for in-space restarts; these are typically reserved for expensive government-owned reconnaissance, communications, or command & control satellites. For existing rideshare launch opportunities, nano-scale spacecraft are delivered to orbit as passive payloads and must accept whatever orbit they achieve during the deployment process. Secondary payloads, especially in the nanosat class, with little or no ability determine their deployment orbit, will remain a novelty with little means to accomplish serious scientific, strategic, or commercial missions.

Finally, even when flown as secondary payloads, NanoSat launch costs are extremely high and are commercially prohibitive. Current launch costs are high for a variety of reasons, with human and environmental safety concerns being very high on this list. Clearly, a dedicated Nanosat launch vehicle is required to reduce costs and provide the required LEO access for NanoSats to achieve practical utility. This vehicle design must address the issues that make traditional launch costs so prohibitive. The activity to be reported by this paper was initiated in response to this nano-launch challenge. Restartable, high performing launch vehicle stages in the 25-250 kg payload size class are not currently commercially available. The proposed hybrid "green-propellant" systems offer significant advantages over competing technologies in the areas of cost, safety, and mission capability. The resulting technology will fulfill the ever-growing mission demands of the extensive NanoSat market by enabling dedicated launch for CubeSat scale payloads.

On the need for reduced hazard space-propulsion propellants

Hydrazine (N_2H_4) has been the standard for in-space propulsion for more than 50 years, and is by far the most commonly used monopropellant for primary spacecraft propulsion and attitude control thrusters. Hydrazine thrusters are simple, versatile, and dependable. Hydrazine is attractive as a spacecraft monopropellant because of its high hydrogen content. When passed through a catalyst the decomposition produces ammonia, nitrogen, and hydrogen gas.[1] The reaction is highly exothermic and associated gaseous products reach temperatures of exceeding 1300°C. Under realistic operating conditions hydrazine decomposition can produce specific impulse levels exceeding 220 seconds under vacuum conditions. Unfortunately, hydrazine is a powerful reducing agent that poses serious biological and environmental concerns.[2] Hydrazine is extremely destructive to living tissues, and is a known human carcinogen. The US Environmental Protection Agency (EPA) classifies hydrazine as "highly toxic". Hydrazine possesses a high vapor pressure and boils readily at room temperature. Thus, there exists significant risk of respiratory contamination and special servicing procedures that employ full-pressure self-contained atmospheric protective ensemble (SCAPE) suits are required.

Although procedures are in place to allow hydrazine to be managed safely on tightly controlled military reservations and at government-operated launch facilities; the toxicity and explosion potential of hydrazine requires extreme handling precautions that increase operational complexity. Increasingly, with a growing regulatory burden, infrastructure requirements associated with hydrazine transport, storage, servicing, and clean-up of accidental releases are becoming cost prohibitive.[3,4] A recent study,[5,6] by the European Space Agency Space Research and Technology Center (ESTEC) has identified two essential design elements to achieving low cost commercial space access and operations; *1) Reduced production, operational, and transport costs due to lower propellant toxicity and explosion hazards, and 2) Reduced costs due to an overall reduction in subsystems complexity and overall systems interface complexity*. The *ESA/ESTEC* study showed the potential for considerable operational cost savings by simplifying propellant ground handling procedures. Developing a non-toxic, stable "green" alternative for the most commonly used in-space propellant-hydrazine-was highly recommended by the ESTEC study.

Emerging alternatives to hydrazine-based propellants

In response to this recommendation, for the past decade the US Air Force (USAF) and the Swedish Space Corporation (SSC) subsidiary *Ecological Advanced Propulsion Systems* (ECAPS) have been pursuing less hazardous alternatives to hydrazine. The two most highly-developed "green-propellant" alternatives are based on aqueous solutions of the *ionic liquids* (Ils) Ammonium Dinitramide (ADN),[7] and Hydroxylamine Nitrate (*HAN*).[8] However, both of the above-mentioned IL-propellants are toxic to organic tissue, and special handling precautions are required. IL-based propellants are not truly "green." Thus, the USAF has recently begun to refer to such IL-formulations more properly as having "reduced toxicity" properties. Ionic liquids are water-soluble ammonium-salts that normally exist in solid form at room temperature, but melt below the boiling point of water. When dissolved in water these materials exhibit very strong ion-to-ion interactions. The surface charge attractions of these ions act to tightly hold them together in solution, and as a result produce a significantly lowered vapor pressure. This lowered vapor pressure reduces the risk of toxicity posed by any escaped vapor from the monopropellant containment vessel. Spacecraft may be serviced without the use of SCAPE suits.

[1]Perry B. *ESPA: An Inexpensive Ride to Space for Secondary Payloads*. Milsat Magazine; 2012.
[2]Foust J. New Opportunities for Smallsat Launches. The Space Review; 2011.

Citation: Whitmore SA, Armstrong IW, Heiner MC, et al. High-performing hydrogen peroxide hybrid rocket with 3-D printed and extruded ABS fuel. *Aeron Aero Open Access J.* 2018;2(6):334–354. DOI: 10.15406/aaoaj.2018.02.00068

In August 2011, ECAPS announced the results of a year-long series of in-space tests of a 1-N thruster comparing their High Performance Green Propellant (HPGP) Brand Name LMP-103S, to hydrazine on the Prisma spacecraft platform. ECAPS claims that HPGP delivered equivalent–to-superior performance when compared to mono-propellant hydrazine.[11] NASA has recently selected the USAF-developed HAN-based propellant AF-M315E for its "Green Propellant Infusion Mission (GPIM).[12] Unfortunately, in additional to potential toxicity, there exist several key developmental issues associated with IL-based propellants that make them unsuitable for small spacecraft applications. The high water content makes IL-propellants notoriously hard to ignite. Multiple catalyst systems have been developed to augment IL ignitability; however, room temperature ignition does not currently exist. Catalyst beds must be preheated from 350-400°C before and during ignition, and this preheat can consume up to 15,000 joules of energy. Catalyst beds and associated heating systems add significantly to the inert mass of the spacecraft and the high-wattage preheat requirement presents a significant disadvantage for small spacecraft where power budgets are extremely limited. Finally, due to very slow reaction kinetics at moderate pressures (2000-3000 kPa) system latencies associated with IL-based propellants are significant for moderate chamber pressures and may limit the usefulness of IL-propellants for reaction control systems. Clearly, significant technology improvements must occur before IL-based systems can be employed as a primary propulsion unit or as part of the reaction control system for small spacecraft. With the current state of propulsion technology, the only proven non-hazardous propulsion alternative to hydrazine, and available for small ride-share payloads, is based on low-performing cold-gas thrusters.

Hybrid rockets as a green propulsion alternative

The inherent safety and environmental friendliness of hybrid rocket systems have been known for several decades.[14] Hybrids have the potential to act as an ideal "green" alternative to hydrazine. Historically, due to the lack of a reliable non-pyrotechnic, multiple-use ignition method, hybrid rockets have never been seriously considered as feasible for in-space propulsion. However, as will described later in Section III of this paper, this issue has been overcome by leveraging the unique electrical breakdown properties of certain 3-D printed thermoplastics. The associated arc-ignition concept has been developed into a power-efficient ignition system that can be started, stopped, and restarted with a high degree of reliability. Details of this system will be presented in Section III of this report. Hybrid rockets offer particular utility for the upper stages of a nano-launch vehicle. Although a hybrid rocket will increase the overall system dry mass compared to a solid-propellant motor, the capabilities to throttle, shut-down on demand, coast, and relight the motor, will the offset any lost in performance of the stage. Such a "smart- stage" would not only provide ΔV to enable the payload to reach orbit; but can also serve as an on orbit maneuvering system that allows precise placement of the payload.

Finally, orbital debris due to abandoned spacecraft is becoming a huge issue. It likely that United Nations regulations will soon demand active end-of-lifetime deorbit. The system to be investigated here may also provide on-orbit maintenance or end-of-lifetime de-orbit capability.[16]

Previously, the authors of this report have experienced considerable success with small spacecraft systems using gaseous oxygen (GOX) and 3-D printed thermoplastics as the propellants.[17,18] However, GOX was rejected for this upper-stage application due to its low density, required storage pressures, and significant potential for fire hazards when stored in significant quantities at high pressures. Due to its high density, hydrogen peroxide (H_2O_2) was considered to be very promising oxidizer for this application. In order to achieve comparable density to H_2O_2, GOX would need to be stored at pressures above 10,000 psi. During this investigation USU has built a prototype 1/4th scale motor and with a novel non-catalytic ignition system in order to gain experience with using peroxide in hybrid rocket system designs. This paper reports on the development and testing of that prototype system. Primary emphases are placed on ensuring reliable ignition, characterizing performance and enhancing the system performance, and developing regression rate curves.

Hydrogen peroxide as a rocket propellant

Hydrogen peroxide is a powerful oxidizer whose chemical behavior is dominated by the weak nature of the peroxide bond. In pure form H_2O_2 is highly unstable, and very dangerous to work with. Due to its relative instability in pure form, peroxide is typically used in aqueous solutions.[19] Typical mass concentrations include 3-10% for medical applications, and 30%-50% for industrial and agricultural applications. Hydrogen peroxide solutions with mass concentrations greater than 95%-often referred to as high test peroxide (HTP)-have been used extensively for propulsion applications.[20] Hydrogen peroxide readily undergoes a decomposition reaction where both oxidation and reduction occur simultaneously. The stoichiometric decomposition reaction

$$H_2O_2 \rightarrow H_2O + \frac{1}{2}O_2 + heat \quad (1)$$

is very energetic, producing up to 98.1 kJ for every mole of peroxide that is decomposed (2.89 MJ/kg). Figure 1 shows the progress of the decomposition reaction for a 95% HTP solution concentration. Both the *75 KJ/mol* activation energy and *98.1 KJ/mol* decomposition energy are shown on this plot.

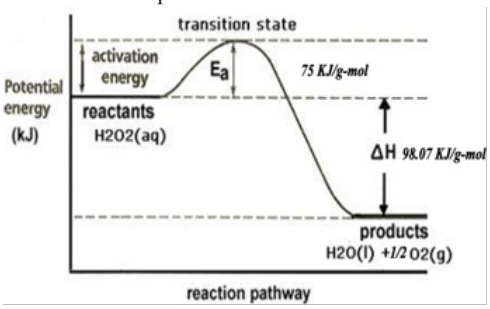

Figure 1 95% Peroxide decomposition energy state with reaction progress.

In typical rocket applications a catalyst bed is used to lower the activation energy for decomposition. A properly-designed catbed lowers the activation energy to the point where a moderate amount of heat can initiate decomposition. As examples, noble metal catalysts like platinum or silver can lower the activation energy to less than 15 kJ/g-mol. Reliable, room temperature, catalytic decomposition typically requires very high concentrations of peroxide, often greater than 95%.[21-23]

At high concentrations H_2O_2 is unstable and slowly decomposes with time. Because of this property, H_2O_2 is typically stored with

a stabilizer in a weakly acidic solution. These stabilizing materials have the detrimental effect of gradually deteriorating any catalyst material in use. This poisoning will eventually render the catbed ineffective. The intense heat of decomposition can also render most catalyst materials ineffective after just a few uses. Because they are constructed from very expensive noble metals, the associated limited use lifetime makes catalyst beds quite expensive to build and maintain. Additional drawbacks include a significant catbed weight that contributes nothing to propulsive mass of the system. Also, even at very high concentrations, a significant pre-heat of the catalyst bed is required prior to the initiation of the peroxide flow. Such a pre-heat may require energy and mass budgets that are not feasible for on-orbit operations. This combination of factors makes the use of catbeds energy and mass inefficient. Their required use drives operating costs up, potentially to the point of being cost prohibitive for small systems requiring multiple reliable restarts.

Monopropellant peroxide performance

When used as a monopropellant, the performance of an aqueous H_2O_2 solution drops rapidly as the solutions mass concentration becomes increasingly more dilute. Figure 2a illustrates this monopropellant performance drop off where the characteristic velocity,

$$c^* = \frac{P_0 A^*}{\dot{m}_{total}} \quad (2)$$

is plotted as a function of the percentage H_2O_2 mass concentration. In Eq. (2) c^* is the characteristic velocity, P_0 is the combustion chamber pressure at which decomposition occurs, A^* is the equivalent choke-point cross sectional area, and $\dot{m}_{total}$ is the monopropellant massflow rate. Figure 2b also plots the predicted decomposition temperature as a function of mass concentration. The presented data was calculated using the industry standard NASA chemical equilibrium code CEA.[24] The calculation assumes a 100% decomposition efficiency. The monopropellant characteristic velocity drops nearly linearly with mass concentration, and over the range from 80% to 100%, c^* drops by approximately *13.5 m/sec* for each % of mass-dilution. At concentrations below 63.8% there is insufficient decomposition energy to boil away all of the water in the solution; thus, the temperature becomes fixed at 100°C.

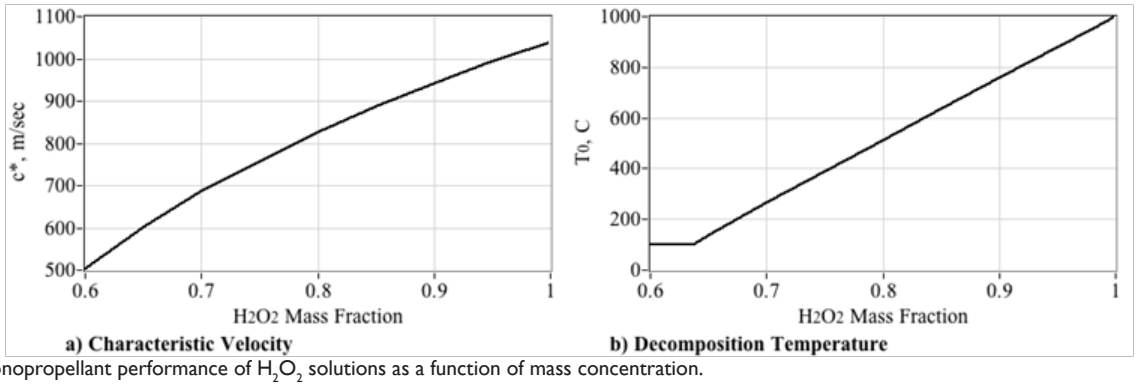

Figure 2 Monopropellant performance of H_2O_2 solutions as a function of mass concentration.

Peroxide hybrid rocket performance

When used as a hybrid bipropellant, in contrast to monopropellant applications, hydrogen peroxide does not exhibit this dramatic performance drop off with mass concentration. Figure 3 shows this property where peroxide is combined with a common 3-D printable thermoplastic, acrylonitrile butadiene styrene (*ABS*) as hybrid propellants. Plotted in 3(a) is the characteristic velocity as a function of the H_2O_2 solution (*oxidizer*) to consumed ABS (*fuel*) ratio (*O/F*). These calculations were performed using the NASA CEA code,[24] assuming a range of combustion pressures of from *1000 kpa (145 psia)* to *5000 kpa (725 psia)*. This equilibrium calculation also assumes that sufficient energy is available to initiate the propellant combustion.

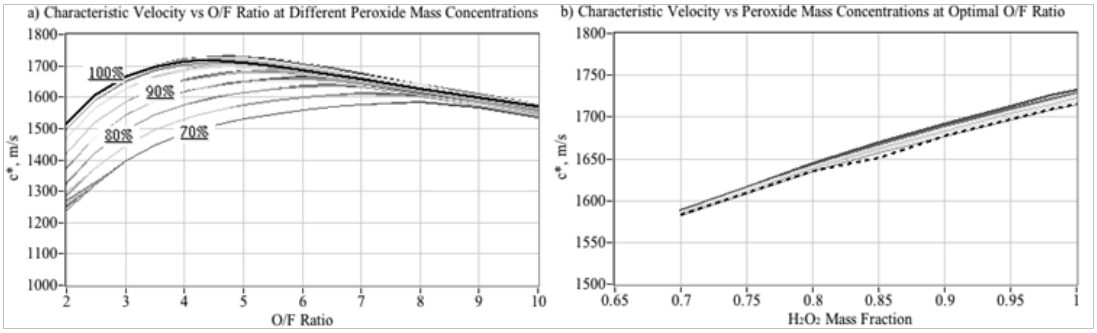

Figure 3 Hybrid performance of H_2O_2 as a function of solution mass concentration.

Note that at 90% concentration the hybrid characteristic velocity is only approximately 2% lower than occurs with a 100% solution concentration. For an 85% peroxide mass concentration the corresponding c^* value drops by approximately 5%. These hybrid propellant c^* drops are contrasted with drops of 22% and 50% for 90% and 80% monopropellant peroxide. In fact, due to its high specific gravity, hydrogen peroxide appears to be an ideal hybrid oxidizer for systems where volumetric efficiency is of primary importance, as in small spacecraft applications. To illustrate this volumetric efficiency, Figure 4 compares the performances of 4 different hybrid propellant

Citation: Whitmore SA, Armstrong IW, Heiner MC, et al. High-performing hydrogen peroxide hybrid rocket with 3-D printed and extruded ABS fuel. *Aeron Aero Open Access J.* 2018;2(6):334–354. DOI: 10.15406/aaoaj.2018.02.00068

combinations. These propellant combinations are *GOX/ABS*, liquid oxygen *(LOX)/ABS*, nitrous oxide *(N_2O)/ABS*, and *90% H_2O_2/ABS*. Plotted are (a) characteristic velocity c^*, (b) effective specific gravity Sg, (c) vacuum specific impulse I_{sp}, and (d) density specific impulse ρ_{Isp}. These calculations were performed assuming a combustion pressure of *1500 kpa (217 psia)*.

The effective specific gravity of the propellants is calculated as the mass weighted averages of the component densities (ρ_{ox}, ρ_{fuel}) and the combustion oxidizer-to-fuel ratio *(O/F)*, divided by the standard density of water

$$S_g = \left(\frac{\rho_{ox}\rho_{fuel}}{\rho_{H_2O\,std}} \right) \quad (3)$$

The vacuum specific impulse calculations assume a 25:1 nozzle expansion ratio. At 90% mass concentration, the peroxide/ABS combination offers a significant improvement in volumetric efficiency compared to the other "green" hybrid oxidizers {*GOX, LOX, and N_2O*} with a peak mass-density specific impulse 25% higher than *LOX/ABS*, and more than three times higher than *GOX/ABS*. Two key insights can be gathered from the data presented by Figure 2, Figure 3, and Figure 4. First, hybrid *H_2O_2/ABS* propellants have the potential to deliver significantly higher c^* and a corresponding increase in specific impulse (I_{sp}) than does monopropellant peroxide. Second, lowering the peroxide mass concentration for the hybrid does not hurt the equilibrium performance nearly as much as it does when peroxide is used as a monopropellant.

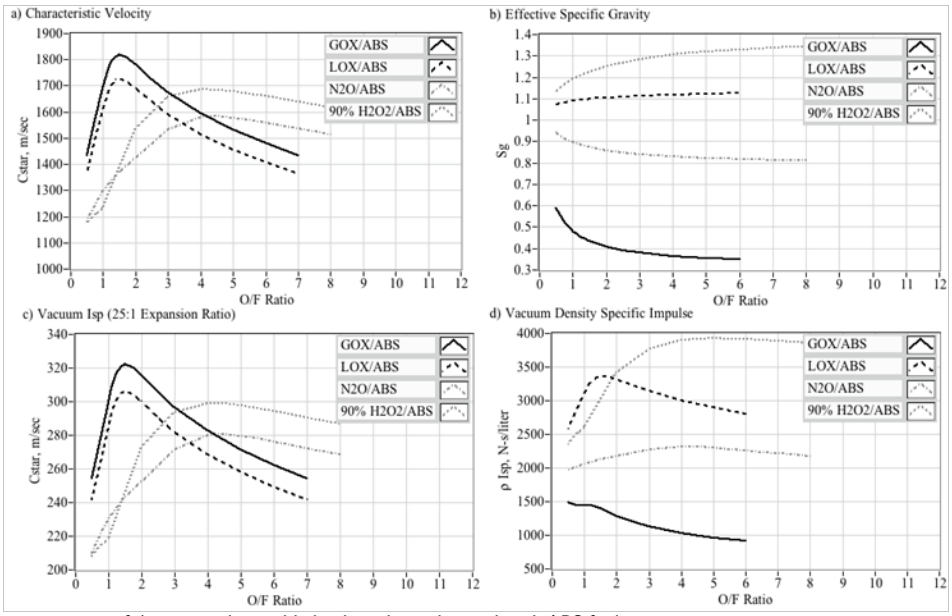

Figure 4 Performance comparisons of 4 commonly used hybrid oxidizers burned with ABS fuel.

Reduction of Risk with 90% Peroxide

The "forgiving" nature of peroxide concentration with regard to hybrid combustion performance is quite significant from an operational point of view. The high test peroxides (HTP) required for monopropellant applications, with concentrations greater than 95%, are registered by the US Department of Transportation under the Code of Federal Regulations (CFR) as a Class 4 oxidizer, and as a DOT Class 4 unstable material.[25] As a class 4 oxidizer HTP can cause explosive reactions due to contamination or exposure to thermal or physical shock. Additionally, the oxidizer will enhance the burning rate and may cause spontaneous ignition of combustibles. HTP is corrosive and "burns" skin and tissue upon contact. HTP can initiate decomposition of materials which in themselves are not likely to undergo explosive decomposition because they require a strong initiating source. HTP is an extremely dangerous material to work with. Storage of large quantities presents a significant explosion hazard. Regulations regarding the sale, use, transport, and storage of DOT Class 4 oxidizers are extremely stringent. By contrast, at concentrations of 90% or lower, the propellant is reduced in hazard to a class 3 oxidizer. Regulations regarding the sale, use, transport, and storage of DOT Class 3 oxidizers are significantly less stringent than for DOT Class 4 oxidizers. These features offer the potential of developing a high performing system, but with a significantly lowered operating risk and a significantly a reduced regulatory burden. Thus, there exists a potential for significant costs savings.

Peroxide catbed design efficiency considerations for hybrid rockets

The efficiency of the catbed has a significant effect on the decomposition temperature; thus, choosing appropriate catbed geometry is critical in order to avoid a "wet start" that may affect ignitability of the system. The general non-efficient reaction for catalytic decomposition of peroxide is written as

$$H_2O_2 + \left[\left(\frac{1-f}{\eta . f} \right) . \left(\frac{M_{w_{H_2O_2}}}{M_{w_{H_2O}}} \right) \right] H_2O = H_2O + \frac{1}{2}O_2 + \left[\left(\frac{1-f}{\eta . f} \right) . \left(\frac{M_{w_{H_2O_2}}}{M_{w_{H_2O}}} \right) \right] H_2O + \left[\frac{1-\eta}{\eta} \right] H_2O_2 \quad (4)$$

where, f is the peroxide mass fraction in the solution, η is the decomposition efficiency, and the M_w's are the respective molecular weights of peroxide, *34.01 kg/kg-mol*, and water, *18.02 kg/kg-mol*. Inspection of Eq. (3) shows that the "effective" solution mass ratio for inefficient decomposition is

$$\frac{M_{H_2O_2}}{M_{H_2O_2}+M_{H_2O}} = \frac{1}{1+\frac{M_{H_2O}}{M_{H_2O_2}}} = \frac{1}{1+\left(\frac{M_{wH_2O}}{M_{wH_2O_2}}\right)\left(\frac{m_{H_2O}}{m_{H_2O_2}}\right)} = \frac{1}{1+\left(\frac{M_{wH_2O}}{M_{wH_2O_2}}\right)\left(\left(\frac{1-f}{\eta.f}\right)\left(\frac{M_{wH_2O}}{M_{wH_2O_2}}\right)\right)} = \frac{\eta.f}{1-(\eta-1).f} \quad (5)$$

Using Eq. (5) and the data of Figure 2, Figure 5 plots the predicted peroxide plume temperatures as a function of decomposition efficiency and peroxide concentration.

For example, Figure 5 shows that a 90% peroxide solution with *η=100%* decomposition efficiency results in a decomposition temperature of approximately 756˚C. However, when the decomposition efficiency reduces to 90%, the resulting decomposition temperature drops to only 370˚C. When 90% peroxide is decomposed at 80% efficiency, the decomposition does not provide sufficient heating rate to vaporize all of the water in the solution, and the temperature rises to only 100˚C. Even at 95% decomposition efficiency, the plume exiting the catbed barely exceeds 500˚*C* for a 90% peroxide solution.

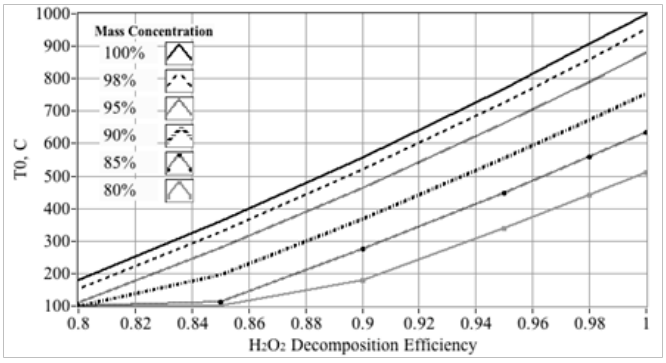

Figure 5 Estimated peroxide decomposition temperature as a function of Catbed η and f.

Effects of H_2O_2 plume expansion entering hybrid combustion chamber

Assuming a typical in-line configuration where the catalyst bed lies upstream of the hybrid combustor; as the plume enters the cold combustion chamber, it instantaneously expands to ambient conditions. This expansion super cools the decomposition products, potentially dropping the temperatures to levels that are below the pyrolysis temperatures of the fuel. The data plotted on Figure 6 quantify this phenomenon. Here the decomposed peroxide plume temperature T_0, entering the combustion chamber is taken from the data of Figure 5. Then assuming an adiabatic expansion from the catbed exit pressure P_{atbed}, to the local chamber pressure $P_{chamber}$, the pre-combustion chamber temperatures are calculated by assuming an adiabatic expansion,

$$\frac{T_{Chamber}}{T_0} = \left(\frac{P_{Chamber}}{P_{catbed}}\right)^{\frac{\gamma-1}{\gamma}} \quad (6)$$

Figure 6a plots the H_2O_2 plume pre-combustion temperature $T_{chamber}$, at various catbed to chamber pressure ratios $P_{chamber}/P_{catbed}$, for a 90% solution concentration. Curves for *{100%, 98%, 95%, 93%, 90%, and 85%}* decomposition efficiencies are plotted. Also plotted are the pyrolysis temperatures for a typical ABS blend,[26] (380˚*C*) and the Arco R-45M[27] HTPB formulation. (430˚*C*). Figure 6b repeats the calculations for an 87.5% solution concentration.

Clearly, the peroxide injection temperatures drop very quickly as the plume expands into the combustion chamber. Once the pressure ratio drops below the choke point, approximately $P_{chamber}/P_{catbed} \leq 0.55$ for 90% peroxide, then a decomposition efficiency of near 93% is required to maintain the chamber temperature above the pyrolysis temperature of ABS. Once the plume temperature drops below this pyrolysis point, then hybrid ignition is nearly impossible. For example, assuming a catbed exit pressure of *250 psia*, then under steady flow conditions and perfect decomposition efficiency of a 90% solution, the fuel pyrolysis is not reached until the chamber pressure exceeds 30 psia. At 95% decomposition efficiency, a chamber pressure of 80 psia would be required to keep the entering plume temperature above the pyrolysis point. Without fuel pyrolysis, then full hybrid combustion cannot begin. At even lower decomposition efficiencies, as often occur when the flow is first initiated into a cold motor, then the plume entering the combustion chamber cools sufficiently to allow the decomposed water vapor to re-condense into liquid form. Such a "soaked" fuel grain would be virtually impossible to ignite.

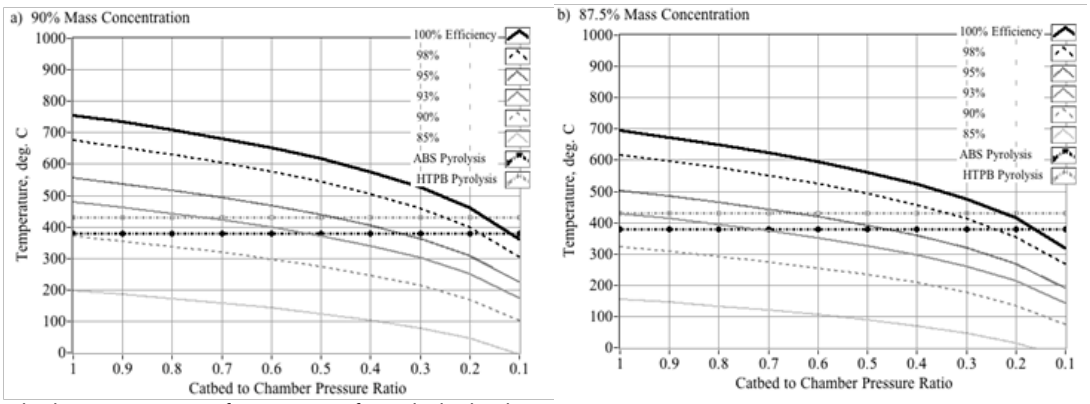

Figure 6 Peroxide plume temperature after expansion for multiple chamber pressure ratios.

Previous applications of hydrogen peroxide in hybrid rockets

Recently, several groups and organizations including the Bloodhound SSC (OK)[3] supersonic car team, ONERA (France),[28] and Nammo Raufoss (Norway),[29] and have tested H_2O_2 as an oxidizer in hybrid rocket systems. These projects have all experienced varying degrees of success, while exhibiting some major technology gaps that still allow considerable room for improvement. Especially at larger scales, a difficulty with ignition and long ignition transients appear to be endemic to the application. The UK Bloodhound team is developing

[3]Anon. How to Build a 1,000 mph Car. The Economist; 2011.

a hybrid rocket motor using HTP (98%) and the legacy solid rocket binder material, Hydroxyl Terminated Polybutadiene (HTPB), as propellants for its supersonic car design. This team has experienced considerably difficulty with getting their motor to light reliably and has resorted to "doping" the fuel grain with ammonium perchlorate (AP) in order to achieve and sustain ignition. This oxidizer addition to the fuel material has resulted in motor stability problems as well as difficulties extinguishing the motor after ignition.

The ONERA motor design relies on both pyrotechnic ignition and catalytic decomposition with swirl injection for ignition. The pyrotechnic ignition was able to successfully ignite the system using lower grade (87.5%) peroxide. However, the catalytic system, based on a silver-screen catbed, required the use of 98% HTP. For both ONERA configurations, static test firings demonstrated considerable difficulty with initiating combustion when using a solid cone nozzle that produced a central flow distribution with very coarse fluid droplets. Instead the ONERA investigators found that combustion efficiency was considerably enhanced using a hollow cone injector nozzle. The hollow cone pattern produced the finest level of atomization with no central flow distribution. Ignition latencies as long as 2 seconds were observed for the catalytic ignition system. The pyrotechnic ignition system reduced the latencies, but was "single-shot" and did not allow for re-ignition of the motor. The ESA-funded Nammo Raufoss (Project) has been ongoing since 2003, and is currently the most accomplished of the existing peroxide-hybrid programs. The Nammo design used HTPB as the accompanying. For this design the peroxide solution was decomposed using SAAB's proprietary catalyst bed design, with the resulting hot gasses injected into the combustion chamber through a vortex injector. The catalyst bed hybrid was able to work with peroxide concentrations as low as 87.5%, but the catbed was quite large and made up a considerable fraction of the overall inert motor weight.

For the typical Nammo motor ignition sequence, after peroxide flow is initiated the chamber pressure gradual builds up from ambient to a plateau at approximately 1500 kPa (220 psia). This "smoldering" buildup of chamber pressure takes slightly more than 2 seconds, followed a sharp rise in chamber pressure to approximately 2500 kPa bars (360 psia). NAMMO refers to the initial pressure buildup as the "*mono-propellant combustion mode*." and the sharp rise and subsequent plateau as "*hybrid combustion mode*." The previously-described expansion and adiabatic cooling phenomena are very likely the reasons for the large ignition latencies and the self-described "*monopropellant*" combustion modes experienced by the NAMMO hybrid motors.[29] At 100% efficiency the decomposition temperature is only *695˚C*. Taking temperature data from Figure 6b for 87.5% peroxide corrected for adiabatic expansion, in order to exceed pyrolysis temperature of their HTPB fuel (*430˚C*) at 95% decomposition efficiency, the chamber-to-catbed pressure ratio needs to at least 0.6. This results is precisely the pressure ratio (*1500 kPa/2500 kPa*) at threshold where the Nammo motor transitions from "*monopropellant*" to "*hybrid*" combustion mode.

Development of a low-energy, non-pyrotechnic, thermal ignition system for H_2O_2/ABS hybrid rockets

Based on the discussion of the previous section, the authors have concluded that unless very high concentrations of peroxide are used, catalytic methods for peroxide hybrid motors will always result in less than satisfactory ignition properties, with substantial ignition latencies. Legacy piled screen-mesh noble-metal catbed designs[30] developed for very high peroxide mass concentrations (98%), are generally ineffective for mass concentrations of 90% or lower. Without an excessive length dimension, the piled screen-mesh design is simply not sufficiently active to allow the decomposition temperatures necessary for igniting the hybrid motor.

Thermal decomposition ignition methods

Instead, this project has emphasized the development of an alternative non-catalytic ignition method to initiate combustion. The alternative method is based on controlled thermal decomposition. In thermal decomposition sufficient heat to overcome the activation energy, depicted by Figure 1, is provided by an external source. The decomposed peroxide releases a large amount of energy that subsequently pyrolyzes the hybrid fuel. Decomposition also liberates a significant volume of gaseous oxygen that in turn burns with the pyrolized fuel. Thermal decomposition of H_2O_2 is a complex process, and involves many intermediate steps including radical species. Although several authors have attempted to model this process with varying degrees of success,[31-33] there is no generally accepted time-accurate model for the solutions with varying mass concentrations. Prior to the results to be reported in this study, restartable thermal decomposition methods for HTP hybrids have never been fully-successful. Previous thermal decomposition methods have involved pyrotechnics where a large enthalpy rate is input in order to overcome the activation energy barrier. This approach presents a significant risk of an uncontrolled reaction. An uncontrolled reaction produces a large quantity of heat and the associated large volumes by-product gases. This sequence of events presents a significant explosion potential. Only, if the rate of thermal decomposition can be precisely controlled, will thermal decomposition produce a viable alternative to catalysis.

Review of electrical arc-ignition technology

The alternative-ignition approach to be presented here leverages the patented arc-ignition system developed for hybrid rockets by Utah State University.[34,35] The arc-ignition technology derives from the electrical breakdown

properties of certain 3-D printed thermoplastics like Acrylonitrile Butadiene Styrene (ABS), Low Density Polyethylene (LDPE) and High-Impact-Polystyrene (HIPS). These properties were discovered serendipitously while investigating the thermodynamic performance of ABS as a hybrid rocket fuel.[36] Figure 7 shows an additively manufactured example of an ABS fuel grain with built in ignitor geometry. Pictured is the pre-combustion chamber that features two impingement shelves intended to trap and mix the injected oxidizer with the pyrolyzed fuel. Two electrodes, insulated by industry standard ESC connectors,[4] are embedded into the top face of the fuel grain. Dual redundant, solid-core copper wires are routed from the electrodes to small gaps located on the impingement shelves. The wires are insulated and protected from flame by 3-D printed circular "slots" that insert into the electrode wire gaps. The conducting paths terminate facing each other, flush with the combustion port surface, and exposed to the interior of the combustion chamber.

When an electrostatic potential is placed across the electrodes, charges flow from the energized electrode causing a localized

[4]Anon. Motor to ESC Connectors; 2017.

electrostatic breakdown of the fuel material. This breakdown allows the charges to carve a path through the material. The resulting arc-track completes the circuit path to return electrode.[37] Current flowing through the material causes Joule heating and pyrolyzes some of the material hydrocarbons. Ignition of the pyrolized fuel vapors occurs as soon as oxidizer flow is initiated. The initial arc-track can be pre-set by doping the surface with graphite powder. Once a surface arc-path has been set, graphite doping is no longer required. Depending on the arc-path length, typical impedances across the material between the wire leads lies in the range from *100kΩ* to *2.5 MΩ*. Identical ABS fuel segments made from extruded/machined ABS or similar thermo-plastics do not exhibit the observed arcing properties. Thus, 3-D printing is an essential requirement of the system.

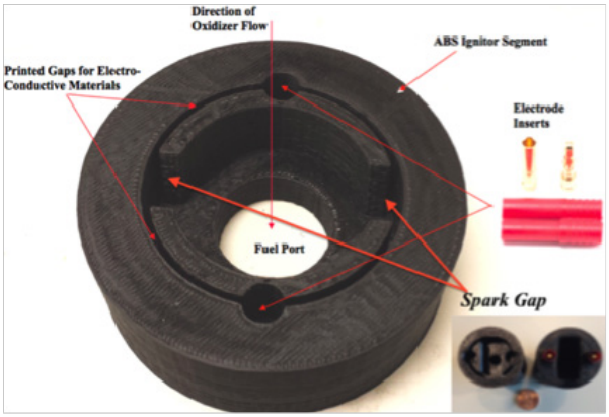

Figure 7 Additively-manufactured fuel grain with integrated electrode paths.

This arc-ignition concept has been engineered into a power-efficient system that can be started, stopped, and restarted with a high degree of reliability. On demand ignition has been demonstrated using compressed air, nitrous oxide (N_2O),[38] gaseous oxygen,[39] and hydrogen peroxide[40] as oxidizers. The arc ignition process is extremely energy efficient, requiring as little as 10 W for less than one second. Typical ignition energies are less than 10 Joules. The arc-ignition system has been demonstrated across a wide range ambient pressures including vacuum conditions.[41] Recently, a small prototype system that burned ABS in enriched air (40% O_2), was spaceflight tested at 170 km altitude. The payload was launched aboard a terrier Malemute launch vehicle from the NASA Wallops Flight Facility. The system successfully performed multiple restarts under hard-vacuum spaceflight conditions.[5]

Thermal decomposition of H2O2 using arc-ignition system

In this approach the peroxide flow is pre-lead by a small flow of gaseous oxygen injected into a combustion chamber lined with the 3-D printed ABS fuel. The arc-ignition system weakly initiates combustion between the injected oxygen and the fuel source, and is followed by the peroxide flow. Previous studies have demonstrated that GOX/ABS combustion generates temperatures exceeding 2800°C, and specific enthalpies greater than *8.5 MJ/kg*. Thus, with the properly tuned GOX pre-lead massflow, there exists sufficient energy to decompose the incoming peroxide flow, while simultaneously initiating full-length hybrid combustion. Once peroxide decomposition begins, then the additional energy of decomposition contributes to the overall combustion process. After the GOX pre-lead is terminated, Combustion is sustained by the oxygen liberated by the thermal decomposition of the peroxide.

Fuel grain design: Previous arc-ignition test prototypes have manufactured the entire fuel grain using 3-D printing. However, due to the associated costs of 3-D printing and the large volume of material that would be required for this testing campaign, only a small ignitor cap section was 3-D printed for each grain. The printed cap was bonded to an extruded ABS rod, machined to fit the appropriate dimensions, to complete the fuel grain. With this change the majority of the fuel grain volume consisted of the significantly cheaper extruded material, as opposed to the 3-D printed material. This approach resulted in considerable cost savings with no reduction in performance. The small 3-D printed cap section provided more than sufficient fuel pyrolysis to seed the flow with hydrocarbon vapor and initiate combustion.

The thrust chamber was developed from a 76 mm hobby-rocket motor case with a graphite nozzle and retainer system. These components were well characterized during a previous research campaign.[42] The ignitor grain segments were manufactured on a Stratasys Dimension® 1200es 3D FDM printer[6] using their standard-grade ABS stock material. The electrodes were manually installed into the assembly and the fuel grains and sealed with the printed "slots" described earlier. The fuel grains were completed by bonding the 3-D printed caps into the lower extruded sections using commercial grade ABS pipe joint cement. The ignitor grain segments were printed fully dense to match the extruded ABS material density of approximately 0.970 g/cm^3. Each ignitor grain segment weighed approximately 110 grams. The ABS grains were machined down to fit the 76 mm chamber from a 3" diameter extruded rod. The bonded grains were press-fit inserted into the motor case with no insulating sleeve. The extruded ABS grain segments weighed approximately 700 grams each. Each completed fuel grain weighed approximately 810 grams. Figure 8 shows the fuel grain and thrust chamber design features.

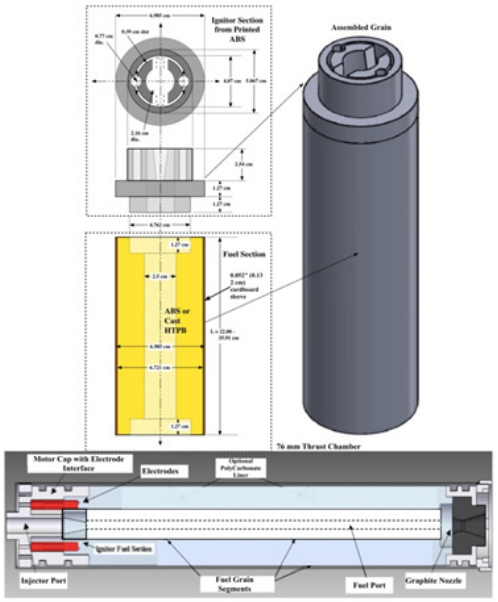

Figure 8 Schematic of 3-D printed Ignitor, extruded ABS lower grain segment, and thrust chamber.

[5]Anon. NASA Launches USU Student-Built Experiment into Space. Prototype Today; 2018.

[6]Anon. Dimension 1200es, Durability Meets Affordability; 2013.

Motor cap and injector designs: Several iterations on the injector cap design, and different injector configurations, were evaluated during this testing campaign. Five different permutations on the H_2O_2 injector were evaluated. In order of test evaluation these components were

a. *Single port injector, custom built from 1/4" NPT brass plugs,*
b. *Five-port straight injector, custom built from 1/4" NPT brass plugs,*
c. *Single port full-cone injector*
d. *Single, large-port hollow-cone, swirl injector,*
e. *Single, small- port hollow-cone, swirl injector.*

Items c) - f) were *Commercial*, *Off-the Shelf* (COTS) Products.

Figure 9 shows the 5 different injector configurations that were tested. Two different GOX injectors configurations were also evaluated. In the initial design the GOX flow was injected asymmetrically through a single port injector. This asymmetrical configuration was found to lead to erosive burning of the fuel grain ignitor section. To correct this issue, the GOX injector was redesigned to use 4 ports, symmetrically arranged around the central peroxide injector outlet. Figure 10 shows the injector cap permutations that were tested during this campaign. Figure 10a shows the original injector cap design, where both the GOX and H_2O_2 lines were attached to the motor cap using NPT fittings. The single orifice was used to feed the propellants into the pre-combustion. Figure 10b shows the modified injector cap with the 4-port GOX injector and the threaded receptacle for the center peroxide injector.

Figure 9 H_2O_2 injector options.

Test motor hardware permutations: Table 1 summarizes the parameters of the tested motor geometry, including the various injector permutations. As a cost saving measure, the test article was mostly assembled from existing parts, and was not optimized for peroxide combustion. After the system was passivated, reassembled, and leak checked, a preliminary set of hot-flow tests were performed to establish the feasibility and assess the effectiveness of arc-ignition system. These initial arc-ignition tests were performed using the single port injector, which proved to be ineffective by allowing a large 2-3 second latency before full ignition was achieved. The single port injector was replaced by a 5-port injector with the same flow cross sectional area. Once again, this injector design was ineffective. Full ignition was finally achieved by replacing the 5-port injector with a full cone injector. Following guidance offered by Anthione et al.,[43] the burn performance was substantially improved by replacing the full-cone peroxide injector by a hollow-cone injector swirl injector. The hollow cone injector performed well; however, the asymmetric GOX injection port lead to erosion and survivability issues with regard to the injector cap section of the fuel grain. Swapping to the 4-port symmetrical GOX injector depicted by Figure 10a greatly reduced the injector cap section erosion and enhanced exhibited the best overall ignition properties, and this configuration was taken forward to the performance Section V of this paper.

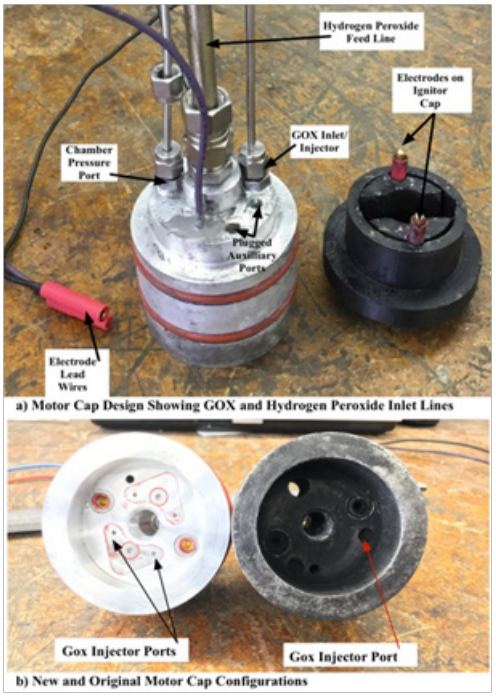

Figure 10 Motor cap configuration with GOX ports.

Description of test apparatus and instrumentation

This section describes the hardware designs and the associated permutations that were used during the development and characterization test phases of this project. As a cost-saving measure, much of the test hard ware used in this campaign was borrowed from previous test articles and adapted for this campaign. By no means are the presented configurations optimized for peroxide combustion.

Ignition system electronics

Figure 11 shows the layout of the arc-ignition system electronics, including the main valve actuation electronics. The ignition system power processing unit (PPU) is based on the UltraVolt® line of high-voltage power supplies (HVPS).[7] This HVPS provides the

[7]Anon. DC-to-HVDC single-output high voltage cap-charging modules. Ultra Volt Inc.; 2018.

inductive ignition spark that pyrolyzes sufficient ABS material to seed combustion. The 30-watt C-series HVPS units take a 15-volt DC input to provide a high voltage output up to 1000 V, with a 30mA current-limit. The entire low-profile HVPS unit weighs approximately *142 grams*, and has dimensions *9.4x3.8x1.96 cm*.

Test stand description

A custom test-stand made from peroxide-compatible materials was built at USU to support peroxide testing activities. Figure 12 shows the Piping and Instrumentation Diagram (P&ID) of the System. Figure 13 shows the cart layout. Except for the N_2 pressurant tank, Figure 13 shows all of the key test components. The instrumentation pallet sits on the lower shelf of the test cart. Figure 13 also shows where the secondary GOX feed line tee'd into the 4-way cross just upstream of the motor. The injector cap lies inside of the pressure thrust chamber pressure vessel and is visible only in the inset image. The system features a 1-liter capacity H_2O_2 run tank pressurized by nitrogen gas with the top-pressure set by a manually-adjustable regulator. A separate 1.5 liter, 2000 psig GOX tank supplies the ignitor flow. Two calibrated venturi flow meters allow direct measurements of both H_2O_2 and GOX massflow rates. The H_2O_2 injector inlet, GOX injector inlet, and the motor head-end (chamber) pressures are also measured. The flow temperature at the H_2O_2 inlet The test sled load structure was fabricated using commercially available aluminum "t-slot." The data acquisition and control system was all contained within a single box mounted to the lower shelf of the test cart.

Table 1 Summary of 76mm test motor geometry parameters

Fuel material	**Outside diameter**	**Port diameter**	**Length**	**Weight**
ABS Ignitor Cap	6.985cm (max) 4.762cm (min)	2.16cm	5.08cm	95.5 grams
Fuel Grain	6.985cm	2.16cm	23cm	800 grams (ABS)
Nozzle	Throat Diameter	Exit Diameter	Exit Angle, deg.	Expansion Ratio
	1.087cm	2.083	12 deg.	3.7:1
GOX	Injector Diameter:	Feed Pressure	Full Tank Pressure	Full Tank Mass
Single Port	0.476cm*	350-500 psig	2200 psig	65 grams
4-Port	4 x 0.238cm*	"	"	"
H_2O_2	Injector Diameter:	Regulator Feed Pressure Settings	N2 Pressurant Tank Pressure	Full Tank Mass
1) Single Port	0.381cm*	350 psig/250 psig	800-1200 psig	525 grams
2) 5-Port	5x0.170cm*	"	"	"
3) Full-Cone	0.254cm, 120 deg spray angle*	"	"	"
4) Hollow-Cone	0.2286cm, 120 deg spray angle*	"	"	"
5) Hollow-Cone	0.1524, 90 deg spray angle*	"	"	"

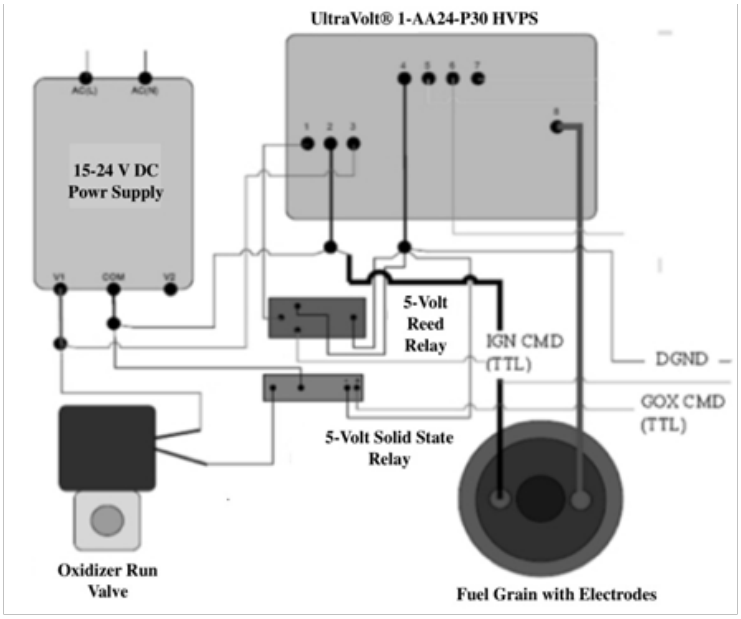

Figure 11 Ignition system electronic schematic.

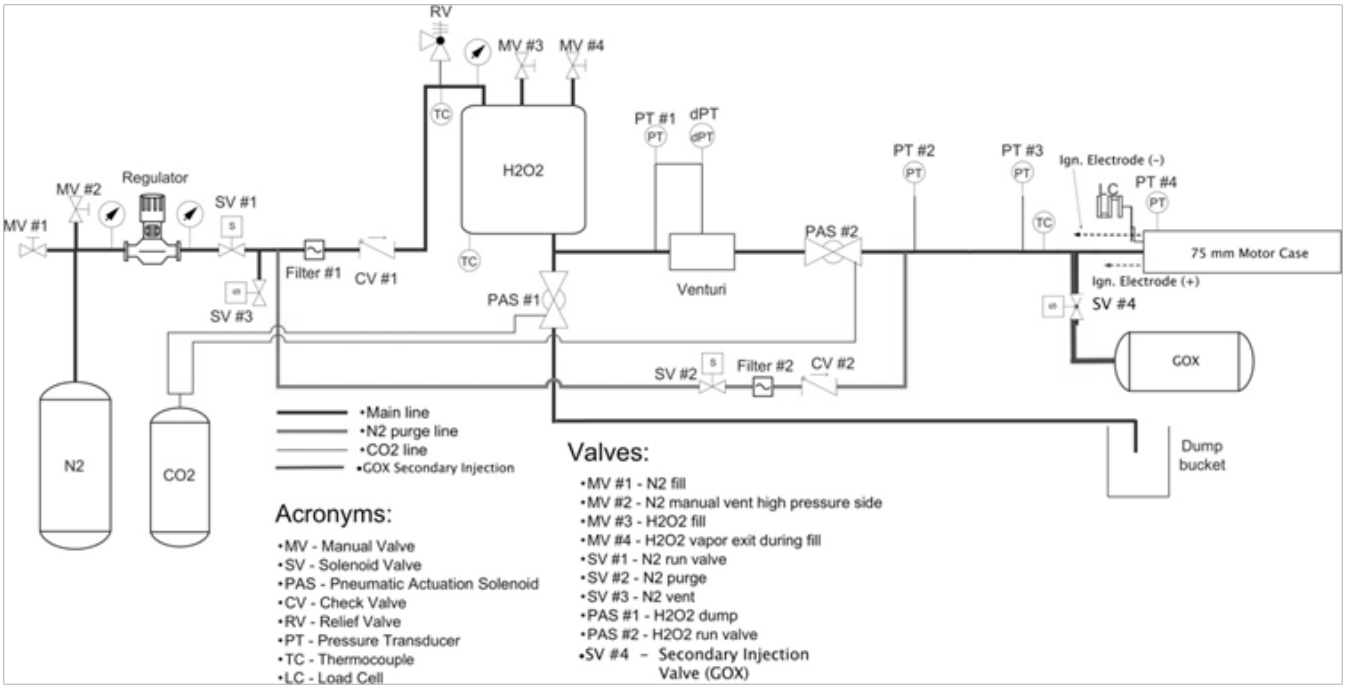

Figure 12 Piping and instrumentation diagram (P&ID) of motor test systems.

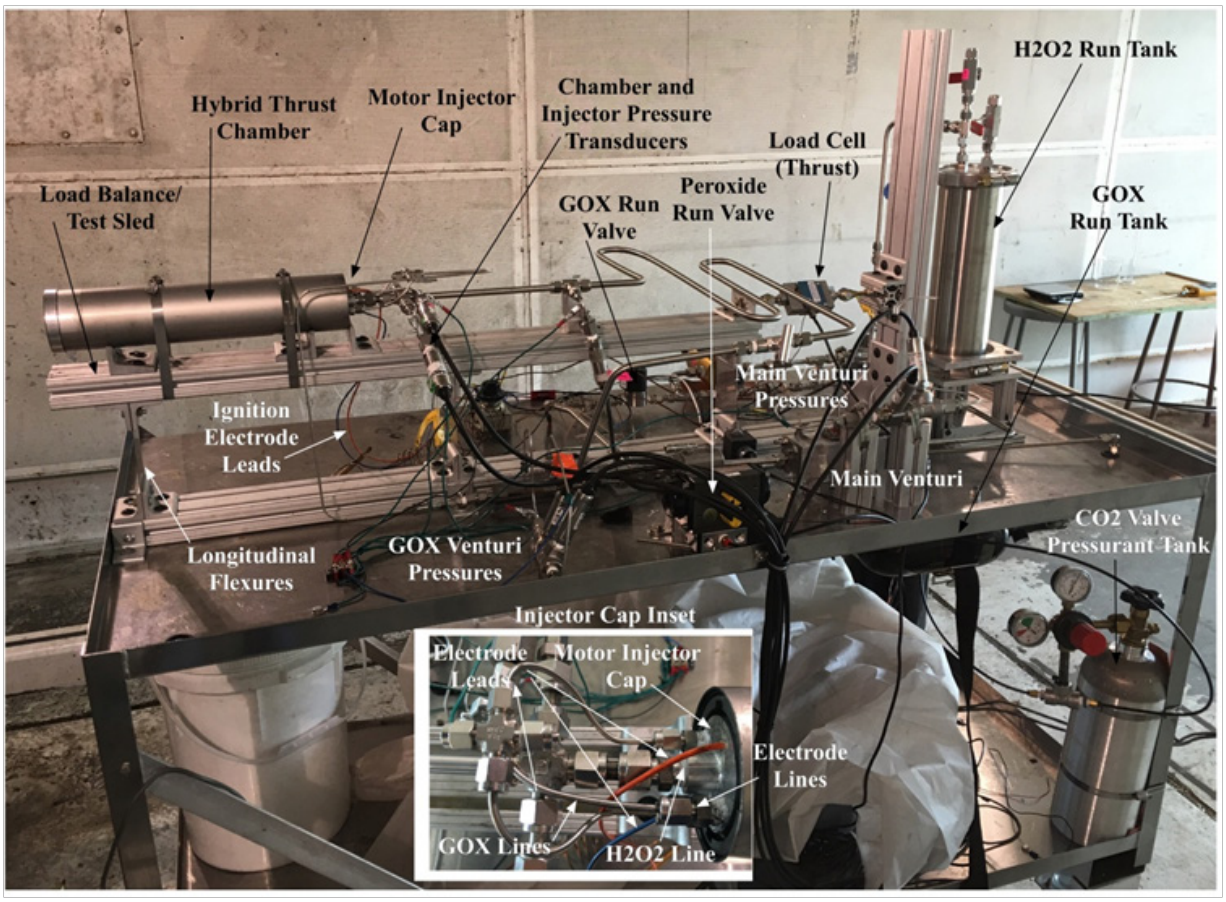

Figure 13 Test stand and instrumentation deck layout.

Citation: Whitmore SA, Armstrong IW, Heiner MC, et al. High-performing hydrogen peroxide hybrid rocket with 3-D printed and extruded ABS fuel. *Aeron Aero Open Access J.* 2018;2(6):334–354. DOI: 10.15406/aaoaj.2018.02.00068

All of the flow path components were chosen for material compatibility with peroxide. Also, each component nominally designed to touch the peroxide flow path was "passivated" prior to the first ground test. The passivating step coats the surface with a thin film of metal-oxide, rendering the surface unreactive with peroxide. Traditional passivation procedures use concentrated nitric acid for passivation, and require many specialized steps not commonly available to small laboratory operators. For this test series the USU Propulsion Research Laboratory relied on data recently published by Yasensky et al.,[44] whereby, a simple passivation procedure using citric acid was demonstrated to be superior to traditional passivation methods as specified by ASM2700E.[45] A commercially-available ultrasonic bath was used to achieve the required constant agitation and control the bath temperature. The recommended citric-acid process worked very well and saved the project several thousand dollars in operating costs. All peroxide tests were performed within USU's on-campus test cell located in the Engineering Technology Building. Two National Instruments data acquisition and control devices manage motor fire control, and test data logging. Operators and experimenters are remotely located in a secure control room separated from the test area. Communications to the test stand are managed by an operator-controlled laptop via universal serial bus (USB) using amplified extension cables. The high flow rate H_2O_2 run valve operated by a CO_2 pressurant tank. The signal to the run valve CO_2 actuator is driven by TTL logic from the controlling laptop. Peroxide and GOX flows are initiated by separate solenoid valves.

Summary of peroxide burn characterization test results

The primary objective of this testing campaign was to demonstrate that hybrid rockets using 90% or less peroxide concentration could be reliably ignited, controllably stopped, and re-ignited. A secondary objective was to characterize the system performance, and to compare those results against existing systems. Finally, the fuel regression rates were measured and curve-fit to develop an engineering model for peroxide/ABS combustion. This model can be used to guide future system designs using these propellants.

Calculating the fuel regression rate for the H2O2/ABS Propellants

Clearly, the effects noted in Figure 22 and Figure 23 are closely tied to the mean regression rate of the solid fuel material burns. Because test stand did include a method for directly sensing the instantaneous fuel mass consumption, the regression rate had to be indirectly inferred from a collection of other mechanical measurements. First, the fuel massflow rate is calculated as the difference between the measured oxidizer (GOX and H_2O_2) and nozzle exit mass flows according to Equation (7),

$$\dot{m}_{fuel} = \dot{m}_{total} - \left(\dot{m}_{GOX} + \dot{m}_{H_2O_2}\right) \quad (7)$$

The instantaneous oxidizer massflow rates were sensed by the calibrated GOX and peroxide venturi flow meters depicted in Figure 12 and Figure 13. The nozzle exit massflow was calculated by the 1-dimensional De Laval choking mass flow equation,[46] using the measured chamber pressure P_0, nozzle exit area A^*, and exhaust gas properties as inputs

$$\dot{m}_{exit} = A^*_{exit} P_0 \sqrt{\left(\frac{\gamma}{R_g . T_0}\right)\left(\frac{2}{\gamma+1}\right)^{\frac{\gamma+1}{\gamma-1}}} \quad (8)$$

In Eq. (8) combustion products for flame temperature T_0, gas constant R_g, and ratio of specific heats γ, were calculated using the method developed by Whitmore and Peterson.[13] In this method tables of the reaction thermodynamic and transport properties were generated with reaction pressure (P_0), oxidizer-to-fuel ratio (O/F), and combustion efficiency (η^*) as independent variables. The combustion efficiency was used to adjust the actual flame temperature compared to the theoretically expected value

$$\eta^* = \sqrt{\frac{T_{0_{actual}}}{T_{0_{ideal}}}} \quad (9)$$

The property tables were constructed using CEA.[24] The enthalpy of formation for ABS used for the CEA tables were generated using Van Krevelin's[47] group addition method, and assuming a 33%, 33%, 34% acrylonitrile, butadiene, and styrene monomer ratios. For this assumed monomer ratio, the effective enthalpy of formation for ABS is calculated to be *64.88 kJ/g-mol*. Separate tables for *GOX/ABS*, *GOX/H_2O_2/ABS*, and *H_2O_2/ABS* reactants were developed, and depending on the states of the run valves, these tables were used to lookup the exhaust property values to be used in the nozzle exit massflow calculations. During the initial GOX-only ignition stages, the *GOX/ABS* lookup tables were used to calculate the flame temperature and combustion properties. During the period where both the GOX and peroxide valves were opened, the *GOX/H_2O_2/ABS* tables were used. Finally, after the GOX valve was closed, the *H_2O_2/ABS* tables were used. The *GOX/H_2O_2/ABS* tables were generated assuming a fixed 12:1 *H_2O_2-to-GOX* massflow ratio.

Using the input values for P_0 and mean O/F, the value of η^* was adjusted to produce a fuel mass flow whose integral over the burn duration matches the consumed fuel mass as measured after each test. Increasing the table lookup input value for η^* has the effect of decreasing the calculated fuel massflow rate, and decreasing η^* has the opposite effect. The longitudinal mean of the fuel regression rate is calculated by dividing the estimated fuel massflow rate by the product of the burn area and the fuel density. The calculation assumes a time-varying fuel port diameter (D_{port}) that is constant along the length of the fuel port (L_{port}).

$$\bar{\dot{r}}(t) = \frac{\dot{m}_{fuel}(\mathrm{t})}{\rho_{fuel}\left(\pi D_{port} L_{port}\right)} \quad (10)$$

The instantaneous (longitudinal mean) fuel port diameter was calculated by integrating the fuel massflow rate, Equation (6) over time

$$D_{port}(\mathrm{t}) = \sqrt{D_0{}^2{}_{port} + \frac{\int_0^t \dot{m}_{fuel}\, dt}{\frac{\pi}{4} L_{port}}} \quad (11)$$

In Eq. (11) D_0 is the fuel port diameter at the start of the burn. Using calculated fuel port diameter and the measured oxidizer massflow rate, the mean longitudinal oxidizer and total massflux are estimated as

Citation: Whitmore SA, Armstrong IW, Heiner MC, et al. High-performing hydrogen peroxide hybrid rocket with 3-D printed and extruded ABS fuel. *Aeron Aero Open Access J.* 2018;2(6):334–354. DOI: 10.15406/aaoaj.2018.02.00068

$$G_{ox}(t) = \frac{\dot{m}_{ox}(\mathrm{t})}{\frac{\pi}{4} D_0{}^2{}_{port}(\mathrm{t})}$$
$$G_{total}(t) = \frac{\dot{m}_{exit}(\mathrm{t})}{\frac{\pi}{4} D_0{}^2{}_{port}(\mathrm{t})} \quad (12)$$

H_2O_2/ABS ARC-ignition hybrid performance assessment tests

As described previously, the initial phase of the development campaign examined various hardware permutation in order to understand the configuration elements that were essential to establishing reliable and repeatable ignition sequences. These early development tests are described in detail by Whitmore et al.,[40] Once the feasibility of achieving reliable arc-ignition was established, the primary focus of the remaining program turned to characterizing the achievable performance of the propellants. For the performance characterization testing campaign each grain was burned multiple times, and the motor disassembled after each test to allow intermediate mass measurements as a check on the accuracy of the real-time measurements.

Table 2 summarizes the results of the ABS characterization tests. A series of 10 ABS-fuel burns using three different fuel grains (multiple burns each) were performed for this testing campaign. Because of the startup transients, where the peroxide enters the motor in still in liquid form; the performance runs were gradually extended from the initial 3 second duration to a length greater than 10 seconds. The longer runs were performed in order to allow the effects of the startup transient to diminish. The first 4-burn set on grain 1 used the asymmetric single-port GOX injector described earlier in this section. The second 4-burn set on grain 2 used the 4-port symmetric GOX injector. All of the first-8 characterization burns used the *0.2286 cm*, *50°* hollow cone peroxide injector. The final two long-duration burns on grain three also used the 4-port GOX injector. The last two burns in this series swapped the original hollow cone injector with a smaller *0.1524 cm*, *90°* hollow cone peroxide injector in order to examine the effects of the reduced injector size on the motor stability. Due to the long burn times, grain 3 could only be safely burned twice without risking motor case burn through.

Table 2 Summary of the Peroxide/ABS burn characterization tests

Burn No. (Grain No.)	Date	Burn Time, s	% H_2O_2 Conc.	Inj. Pf, psia	Chamb. P_c, psia	Thrust, N	Isp, s peak (cumulative)	Port Dia., cm start, (end)	Total Massflow, g/sec	Mfuel burned, g	Mean O/F Ratio	Ign. Energy, J
1 (1)*	9/6/17	2.92	89.4	180	150	122	212(198)	2.45(3.11)	57.7	56	2.038	14.3
2 (1)*	9/8/17	3.11	87	178	148	118	211(196)	3.11(3.29)	56.9	51	2.408	10.2
3 (1)*	9/14/17	2.93	92.4	175	142	114	209(196)	3.3(3.64)	54.6	48	2.698	9.8
4 (1)*	9/21/17	3.14	90.2	177	148	121	210(197)	3.64(3.95)	60.4	88	3.397	7.8
5 (2)**	9/28/17	3.87	90.6	185	152	129	219(201)	2.45(2.67)	59.6	47	2.88	13.2
6 (2)**	10/03/17	7.82	92.4	200	167	138	220(201)	2.67(2.97)	64.2	99	3.386	8.2
7 (2)**	10/06/17	4.11	90.7	195	165	137	218(200)	2.97(3.17)	63.4	57	3.628	6
8 (2)**	10/10/17	3.95	88.7	183	154	125	215(196)	3.17(3.42)	59.2	58	4.219	5.3
9 (3)***	11/02/17	5.88	89.68	200	152	123	213(201)	4.05(4.83)	56.5	87	4.307	12.9
10 (3)***	11/14/17	10.3	91.7	204	157	135	215(201)	4.09(5.08)	61	154	4.18	5.9
Mean (Std Dev.)		4.8 (2.47)	**90.3 (1.6**9)	187.8 (10.7)	153.8 (7.7)	126.2 (8.2)	214.2 (3.9)	N/A	59.4 (3.1)	74.5 (33.6)	3.11 (0.77)	9.3 (3.2)

*Single Port, Asymmetrical GOX Injector, 0.2286cm Hollow Cone 50o Spray Angle Peroxide Injector.
**4-Port Symmetrical GOX Injector, 0.2286cm Hollow Cone 50o Spray Angle Peroxide Injector.
***4-Port Symmetrical GOX Injector, 0.1524cm Hollow Cone 90o Spray Angle Peroxide Injector.

For these performance characterization test the GOX flow time was shortened substantially with a pre-lead before the main valve opening of *1 second*. The GOX valve remained open for *2 seconds* after the main valve was opened. The peroxide valve was opened at time zero, and remained opened until all of the liquid in the peroxide run tank was exhausted. In order to achieve a wider variety of massflux rates during this burn series, the *peroxide* injector feed pressure p_f was varied by manually adjusting the regulator output over a range from 200 to 250 psig. The resulting injector feed pressure varied over a range from 180 to 200 psia, with p_f for the first set of burns on grain 1 averaging approximately 180 psia, and approximately 190 psia for the set of burns on the grain 2. The tabulated O/F ratios were calculated by integrating the oxidizer massflow, and then dividing by the burned fuel mass.

Example burn time histories

Figure 14 and Figure 15 present representative time histories obtained for two longer-duration H_2O_2/*ABS* burn durations. Figure 14 plots the test results obtained using the larger-port hollow-cone injector, and Figure 15 plots the test results obtained using the smaller-port hollow-cone injector. Plotted are (a) directly measured (load cell) thrust and thrust calculated from chamber pressure using the De Laval flow equations, (b) chamber pressure, (c) GOX, peroxide, nozzle exit, and fuel massflow rates, (d) cumulative and instantaneous specific impulse values as calculated using both measured and calculated thrust levels, (e) input power and energy levels, and (f) the oxidizer and total massflux through the fuel port. Figure 16 shows images of a typical complete ignition sequence. The "steady" thrust, chamber

pressure, specific impulse, and injector feed pressures values are calculated as the time-average of all values that are within 95% of the peak value. The cumulative specific impulse is calculated as a running summation of the total impulse and the total consumed propellant mass. This calculation includes the effect of the initial peroxide spike, and will necessarily produce a lower value.

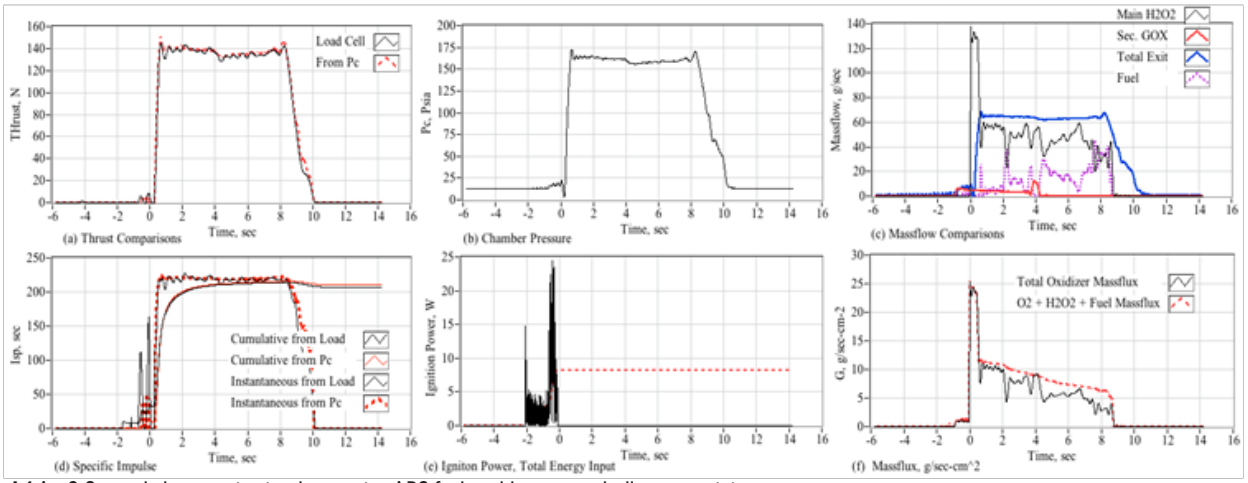

Figure 14 An 8-Second characterization burn using ABS fuel, and large-port hollow cone injector.

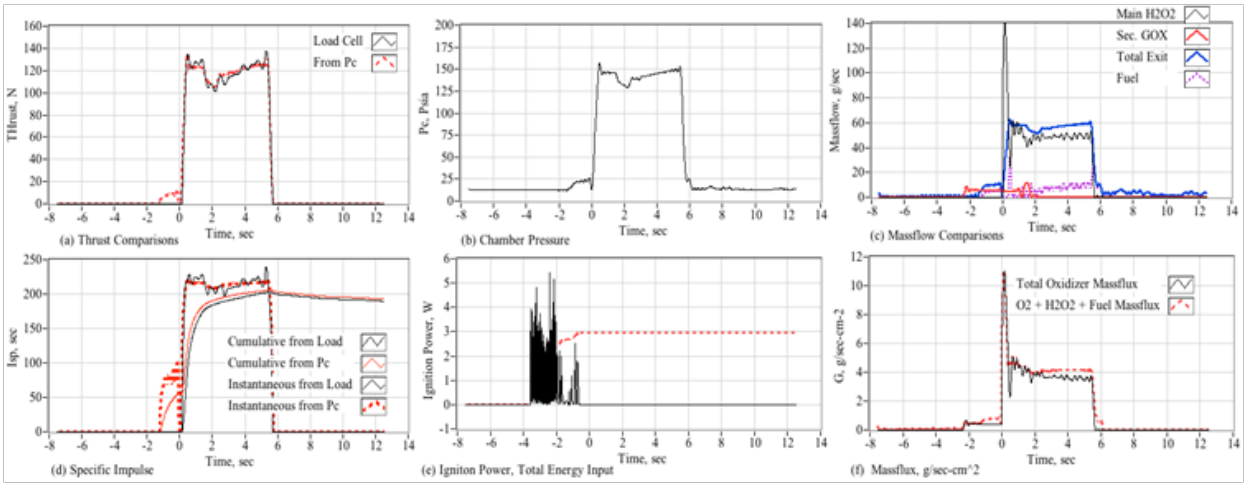

Figure 15 A 6-Second characterization burn using ABS fuel small-port hollow cone injector.

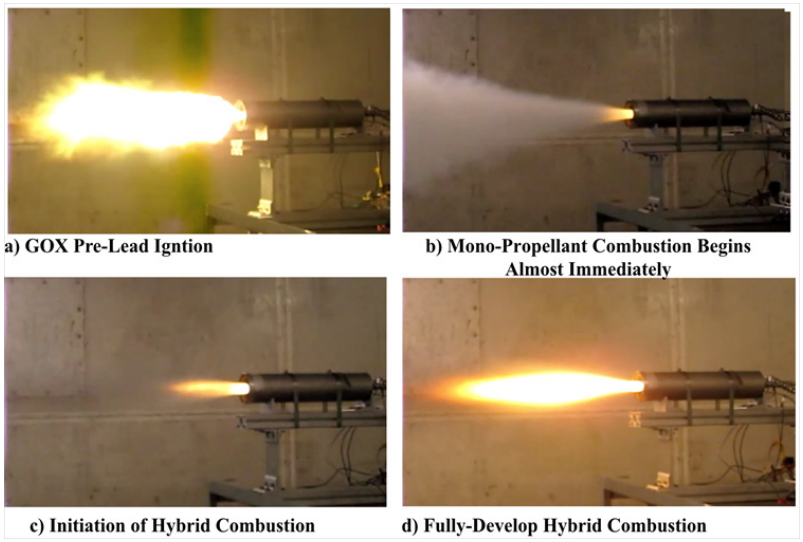

Figure 16 Still images from ignition development test with 50o full-cone main injector.

Citation: Whitmore SA, Armstrong IW, Heiner MC, et al. High-performing hydrogen peroxide hybrid rocket with 3-D printed and extruded ABS fuel. *Aeron Aero Open Access J.* 2018;2(6):334–354. DOI: 10.15406/aaoaj.2018.02.00068

Because of the startup transients, where unburned peroxide floods the combustion chamber during the startup transient, the integrated specific impulse values are consistently lower than the instantaneous values; however, and the burn time increases, the effects of the startup transient diminish and the integrated values begin to catch up with the instantaneous values. The mean and standard deviation values for each parameter are listed in the last row of this table. The methods used for calculating the total nozzle exit and fuel massflow rates were presented earlier in the previous section. Table 2 shows "instantaneous" mean I_{sp} of approximately *212.6 s*, with a standard deviation of *±4.6 s*. The cumulative specific impulse is approximately 196.4 sec, with a standard deviation of *±3.29 s*. The instantaneous value for I_{sp} is calculated by dividing the sensed thrust by the instantaneous nozzle massflow calculated from chamber pressure. The cumulative value for I_{sp} is calculated by integrating the thrust and massflow over time, and dividing the accumulated total impulse by the total mass exited from the nozzle over time. The cumulative I_{sp} includes the "lost mass" due to the *initial transient unburned peroxide transient massflow*.

These ensemble data agree well with the time history traces of Figure 14 and Figure 15 where the instantaneous I_{sp} peaks at a value near *220 s*; and the accumulated falls just short of *200 s* for the shorter burn and lies slightly above *200 s* for the longer burn. Because the effect of the initial transient diminishes with time, the longer duration burn "steady" I_{sp} value is most representative of the performance that would be achieved in an operational setting, where burns longer than 1 minute in duration would be typical. For the short burns, the effect of the initial peroxide flow transient is exaggerated by this calculation. Figure 17 plots the mean *O/F* ratio (a) and the total ignition energy (b) as a function of the accumulated burn time for each fuel grain. Figure 17a shows that the O/F ratio shifts towards a progressively leaner burn as the fuel port opens up and the mean massflux drops. Also noted is the ignition energy dropping with burn time. This observation supports the earlier discussion of current-path impedance dropping as the arc-path sets into the fuel grain. Agreements exhibited between each of the burned fuel grains of Figure 17 are excellent. All 3 fuel grains tended to burn slightly fuel rich, indicating that the motor length was slightly longer than optimal.

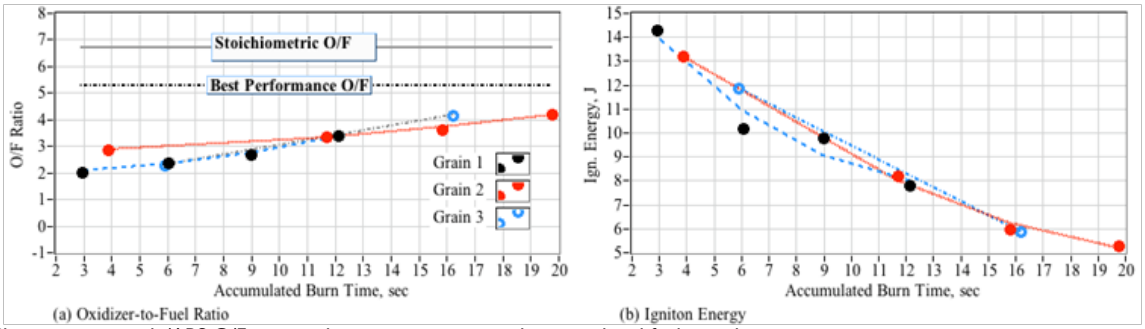

Figure 17 Changes in peroxide/ABS O/F ratio and ignition energy as with accumulated fuel grain burn time.

Fuel regression rate measurements

Because the sensed peroxide flow rate was somewhat erratic,[8] and also due to time phasing differences between the nozzle exit and peroxide massflow rates;[9] the regression rate and mass fluxes as calculated by Eqs.(10) and (12), do not correlate well when plotted against each other. Instead, the regression rate and mass fluxes are integrated over time, and then curve fit using a linear trend line. The resulting slopes are representative of the effective mean regression rates and massflux for the entire burn. Figure 18 shows example regression and massflux trend lines corresponding to the data of Figure 14 and Figure 15. Figure 19 plots the shows the resulting trend lines when the regression and massflux slopes are calculated for each of the test burns of Table 2. Figure 19a plots the calculated regression rate against the mean *oxidizer massflux* rate for each burn of Table 2, and Figure 19b plots the calculated regression rate against the mean *total massflux* rate for each burn of Table 2. The massflux values are calculated using the previous method previously described in section L. Also plotted are the exponential curve-fits (solid lines) of the form

$$\dot{r} = a.G_{ox}^{\ n}$$

$$\dot{r} = a.G_{total}^{\ n} \quad (13)$$

where *{a, n}* are the motor scale constant and burn exponent. The curve fits assume zero regression rate at zero flux level. The 95% confidence-level uncertainty boundaries as calculated using the *student-t* distribution[48] with 9 degrees of freedom, are also plotted as the dashed lines. Table 3 summarizes the results of Figure 19.

Comparisons to previously-obtained ABS regression rate for GOX and N2O

Previously, Whitmore et al.,[49] and Whitmore & Merkley[50] had burned this same 75-mm motor configuration using 3-D printed ABS as the fuel with gaseous oxygen (GOX) as the oxidizer. Also, Whitmore et al.,[36] have tested and compared the performances and mean regression rates of 3-D Printed ABS and HTPB when burned with nitrous oxide. The resulting regression rates from these test campaigns are compared against the data presented by Figure 18 as a "sanity check" of the test methods and results. Figure 20 presents the collected test results where the regression rates and corresponding exponential curve fits are plotted as a function of the oxidizer massflux. The nitrous oxide data were obtained with a significantly larger *800 N, 98-mm* motor; thus, the massflux levels are larger by a factor of approximately 4, than those of the *125 N, 75-mm* motor. Generally, the data exhibit reasonable magnitude agreements, and support the methodology used to calculate the regression rates. All of the massflux values listed by Tables 3 lie within a range where the regression rate is diffusion dominated,[51] and the resulting data should correlate well with Marxman's,[52,53] classical regression rate theory that predicts an exponent value *n=0.8*. As plotted by Figure 19 the resulting burn exponents for *GOX*, H_2O_2, and N_2O with ABS are *{0.3175, 0.5945, and 0.6694}*, respectively. These equate values equate to differences of {86%, 29%, and 18%} from the Marxman theory, respectively.

[8]The erratic H_2O_2 massflow sensed by the main venturi is likely a result of incipient injector feed coupling, and will be discussed later in this section.

[9]The H_2O_2 massflow sensed by the main venturi is approximately 60 cm up stream of the nozzle exit, and impulses can take as long as 100 ms to traverse the entire length of the thrust chamber.

Table 3 Peroxide/ABS burn characterization test regression rate summary

Burn Number	$\dot{r}$ cm/s	G_{ox} $g/s-cm^2$	G_{total} $g/s-cm^2$	Curve Fits	Scale Factor, a	Burn Exponent, n	Uncertainty @ 95% Conf. level. cm/s
1	0.0884	7.653	10.356	vs. G_{ox}	0.02365	0.5945	+0.003(5.1%)
2	0.0694	5.55	7.395				
3	0.0693	6.401	8.25		$\frac{cm^{1+2n}}{g^n s^{1-n}}$		
4	0.0652	5.944	7.771				
5	0.0708	6.444	8.582	vs. G_{total}	0.02068	0.5799	+0.0035(6.0%)
6	0.07	6.436	8.448				
7	0.0597	4.124	5.546				
8	0.0378	2.833	3.55		$\frac{cm^{1+2n}}{g^n s^{1-n}}$		
9	0.0521	2.743	3.806				
10	0.0981	9.411	11.821				
Avg. (Std. Dev.)	0.0619(0.02437)	5.229(2.347)	6.864(3.1168)				

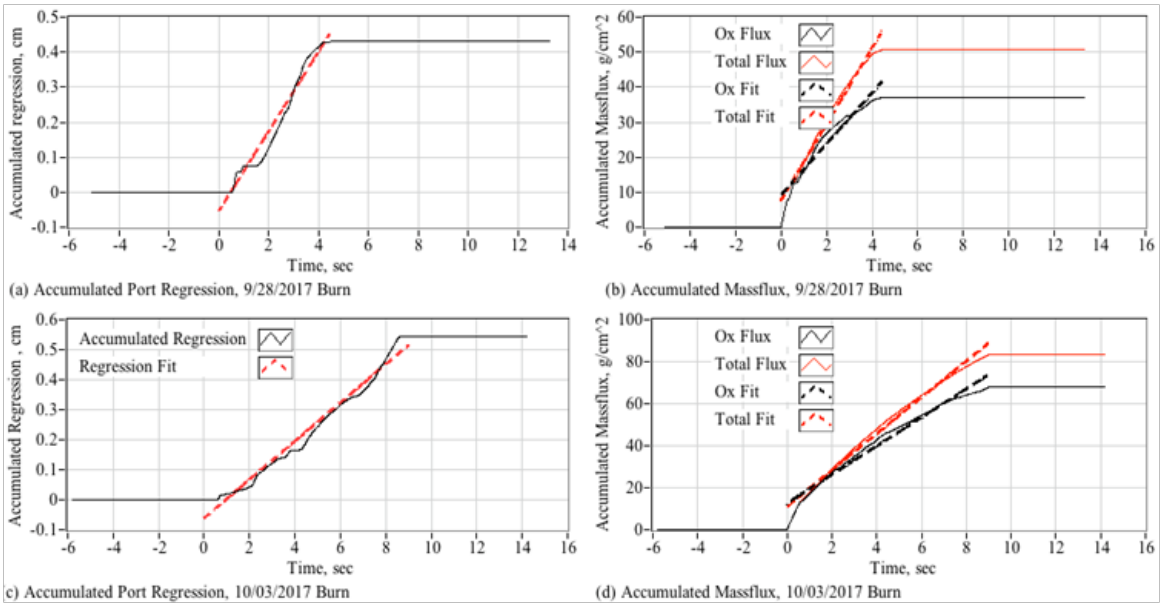

Figure 18 Representative mean regression and massflux time histories for ABS/Peroxide hybrid burns.

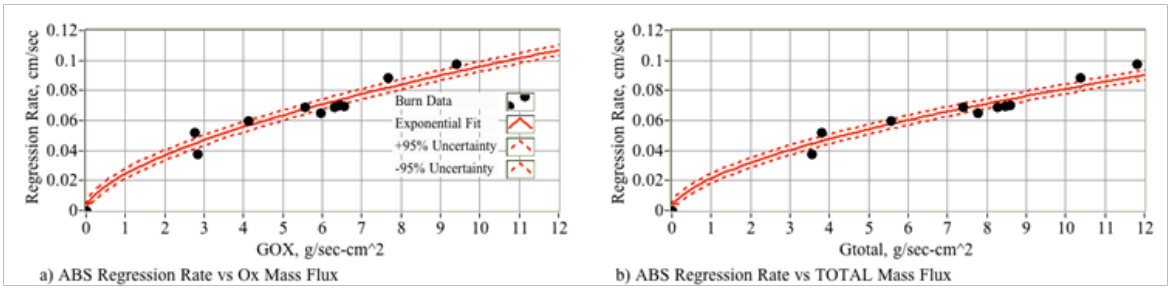

Figure 19 H_2O_2/ABS burn regression rate data, curve fits, and uncertainty boundaries.

Analyses presented by Karabeyogulu[10] for thermosetting fuels like HTPB show that a regression rate exponent value of $n>1/2$ results in a progressive burn pattern with *O/F* ratio increasing as the fuel grain burns and the port opens up. Conversely, when $n<1/2$ the burn pattern is regressive and the *O/F* becomes increasingly fuel-rich with time. An exponent value of $n=1/2$ implies that the burn rate is neutral and no *O/F* shift occurs during the burn. The majority of commonly used hybrid fuels have burn exponents greater than $n=1/2$, and thus the burn becomes increasing leaner with time. As plotted on Figure 17, the H_2O_2/ABS data do indeed exhibit a positive *O/F* Shift as a function of burn time. In contrast the GOX/ABS burn data exhibit a shift towards a lowered O/F ratio, and represent a clear anomaly[50] suggests that radiation heating due to the high temperatures encountered during GOX burns accounts for this observed anomaly. As of this writing, this issue of the differences in the burn patterns caused by the different oxidizers remains unresolved.

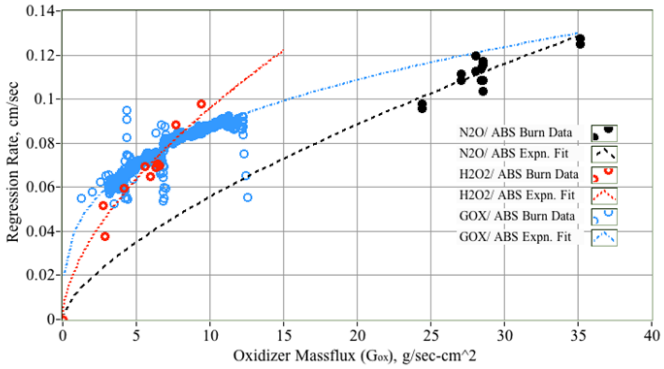

Figure 20 Regression rates for ABS using three different oxidizers: N_2O, H_2O_2, and gaseous O_2.

Effect of peroxide injector pressure drop on motor burn stability

A main common feature to be noted with the ABS fuel burn data of Figure 14 and Figure 15, is the rather more ragged appearances of peroxide massflow curves (c) for data collected using the large-port hollow cone injector. Once the configuration is switched over to the small-port injector, the peroxide massflow rate smooths out considerably. The source of this ragged flow field can be identified by comparing the unfiltered chamber pressure and the resulting chamber frequency spectrum against the massflow curves and the pressure drop across the injector. Figure 21 and Figure 22 present these comparisons for two sample ABS data runs; with the Figure 21 data collected using the large-port injector, and the Figure 21 data collected using the small port injector. In Figure 21a, the unfiltered chamber pressure data exhibit a moderate instability with a chamber pressure cycle of approximately 10-12 psia amplitude. The plotted spectrum of Figure 21b show distinct harmonics at approximately 12 and 40 Hz. These peaks are designated by arrows. Because of the low pressure drop across the injector, about 20-22 psia or only about 11-12% of the feed pressure, there exists an injector feedback coupling that results in the pictured incipient instability, and the resulting unsteady peroxide mass flow rate. Conversely, the data of Figure 22 was measured using the reduced area injector exhibits an injector pressure drop that increases to approximately 50 psia or approximately 33%. This increased pressure drop also significantly improves the motor stability and results in reduced pressure noise levels, and a far more consistent peroxide massflow rate. The 12 Hz harmonic is completely gone, and the 40 Hz harmonic is substantially reduced.

Extrapolating the specific impulse values to hard-vacuum conditions

The graphite nozzle used for this test series exhibited no measurable erosion during the entire characterization campaign. This low erosion rate is very likely due to the slightly fuel rich burns which left no remaining oxygen radicals to combine with the carbon throat. At the chamber pressure levels required for stable motor operation, the nozzle configuration with and expansion ratio of 3.7:1 was slightly over-expanded at the test conditions. The result is a specific impulse approximately 5 seconds lower than would be achieved by the optimal configuration. However, since the nozzle configuration is well known and assuming that a higher expansion ratio has little effect upon the combustion chemistry; this effect can be accounted for, allowing the specific impulse values to be extrapolated to vacuum conditions using data from Table 2. The extrapolation starts with the one-dimensional de-Laval flow equations for a 1-dimensional nozzle[46] fixes the throat geometry and chamber pressures at the values given by Table 1 and Table 2, and adjusts the nozzle exit area (and expansion ratio) to calculate the corresponding exit pressure, thrust, and specific impulse. Table 4 summarizes the results of these calculations. When the nozzle expansion ratio is lowered slightly to adjust the exit pressure upwards to match the ambient conditions, the mean peroxide/ABS specific impulse increases slightly to *217.3 s*, up approximately 1.7% from the mean measured value of Table 2. Finally, when the nozzle exit is opened to a 25:1 expansion ratio, the I_{sp} grows to greater than *300 s*, or about 30% higher than achieved under the actual test conditions.

[10]Karabeyoglu A. Lecture 10 Hybrid Rocket Propulsion Design Issues. AA 284a Advanced Rocket Propulsion, AAE Department, Stanford University; 2012. 18 p.

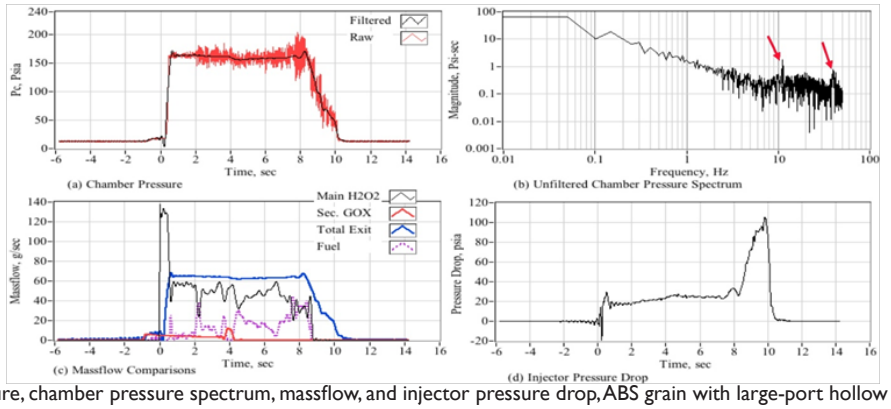

Figure 21 Chamber pressure, chamber pressure spectrum, massflow, and injector pressure drop, ABS grain with large-port hollow cone injector.

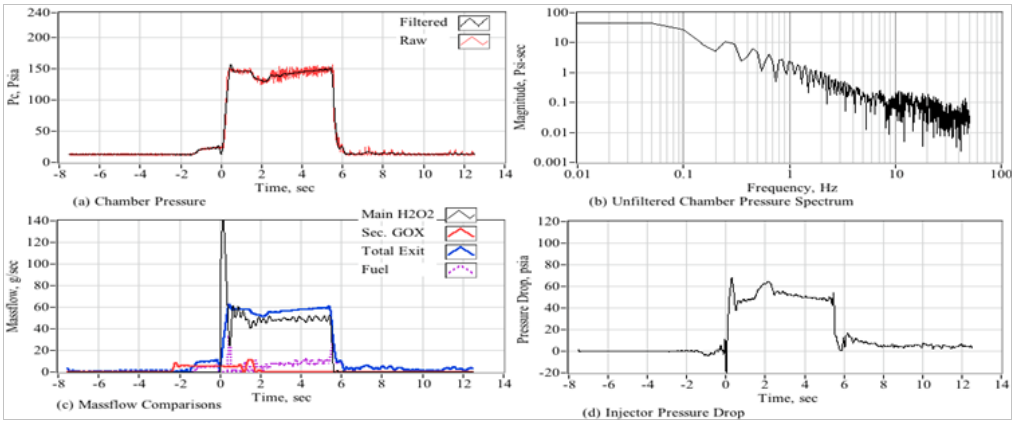

Figure 22 Chamber pressure, chamber pressure spectrum, massflow, and injector pressure drop, ABS grain with small-port hollow cone injector.

Table 4 Extrapolating the test data to optimal and hard vacuum conditions

Condition	Chamber Pressure P_0, *k*Pa (psia)	A^*, cm^2 (in^2)	p_{∞}, *k*Pa (psia)	γ $T_{0\ (K)}$ $R_{g\ (J/kg\text{-}K)}$	A_{exit}/A^*	p_{exit}, *k*Pa (psia)	*1-D Thrust, N*	*1-D* I_{sp}, *s*
Actual test	1060.l (153.76)	0.928	86.82 (12.59)	1.2	3.7:1	52(7.54)	125.2	213.6
Optimal test	1060.l(153.76)			2,720	2.6:1	86.82(12.59)	127.3	217.3
Vacuum	1060.l(153.76)	(0.144)	0	415	25:1	2.21(0.32)	183.1	302.1

Discussion of results

Since a vacuum I_{sp} of *200 s* is approximately 30% higher than can be achieved by hydrazine, the current state of the art propellant for in-space propulsion; the result of the previous section is quite exciting. The issues associated with hydrazine were discussed in the introductory section of this paper. The peroxide/ABS propellants also significantly outperform the ionic-liquid "green" propellants, LMP-103S and AF-M315E; also offering a significantly lower required ignition energy input. Table 5 compares the performance of the peroxide/ABS system to hydrazine, LMP-103S and AFM315-E.[54] The peroxide/ABS system outperforms the other propellants in every measureable category. When fully developed, a peroxide-based hybrid system could revolutionize the commercial space industry by offering a high-performing, but inherently safe, space propulsion option for rideshare payloads.

Table 5 Comparison of propellant performance characteristics[1]

Propellant	**Hydrazine**	**LMP-103S**	**AF-M315E**	**H_2O_2/ABS Hybrid**
Flame Temperature	600-750˚*C*	1600˚*C*	1900˚*C*	2900˚*C*[2]
I_{sp}, *sec*	220-225	252 (theory), 235 (delivered)	266 (theory) 245 (delivered)	324 (theory) 302 (delivered)[3]
Specific Gravity	1.01	1.24	1.465	1.392 (90% H_2O_2)
Density Impulse, *N-sec/ liter*	22705	3125 (theory) 2915 (delivered)	3900(theory) 3650 (delivered)	4450 (theory) 4002 (delivered)
Preheat Temperature	315˚*C*, cold-start capable	300˚*C*	370˚*C*	N/A none-required
Required Ignition Input Energy, *Joules*	N/A	18,000 J (10 Watts @ 1800 seconds)	27,000 J (15 Watts @ 1800 seconds)	2-8 J (8-16 Watts for 250-500msec)
Propellant Freezing Temperature	1-2˚*C*	-7˚*C*	< 0˚*C (forms glass, no freezing point)*	-10˚*C (90% concentration)*
Cost	$	$$$	$$$$	$
Availability	Readily Available	Restricted Access	Limited Access	1Very Widely Available[4]
NFPA 704 Hazard Class			 5	

[1]Data for hydrazine, LMP-103S and AFM315-E were taken from Ref. 54.
[2]Due to the high pyrolysis energy of the ABS fuel, 3.1 MJ/kg, ABS Hybrid motors are self-ablative and do not get hot externally.
[3]Extrapolated to vacuum conditions based on ground test data
[4]80-90% solutions easily condensable from 30% agricultural/food grade solutions.
[5]Based up the constituent components, Hydroxyl Ammonium Nitrate (HAN) and 2-Hydroxyethylhydrazine (HEHN).

Citation: Whitmore SA, Armstrong IW, Heiner MC, et al. High-performing hydrogen peroxide hybrid rocket with 3-D printed and extruded ABS fuel. *Aeron Aero Open Access J.* 2018;2(6):334–354. DOI: 10.15406/aaoaj.2018.02.00068

Conclusion

The Propulsion Research Laboratory at Utah State University has recently initiated development of a novel laboratory hybrid thruster that employs medium grade hydrogen peroxide and additively-manufactured ABS as propellants. The thruster system was adapted from previous hybrid systems previously designed and tested at USU. For this testing campaign, an alternative ignition method that thermally-decomposes the injected H_2O_2 stream is employed. This approach eliminates the need for expensive and mass inefficient catalytic systems. With this novel approach the peroxide flow is pre-lead by a small flow of gaseous oxygen injected into a combustion chamber lined with the 3-D printed ABS fuel. USU's patented arc-ignition system weakly initiates combustion between the injected oxygen and the fuel source, and is followed by the peroxide flow. Released heat from burning fuel is sufficient to initial thermal decomposition of the injected peroxide stream. Heat liberated by thermal decomposition of the peroxide subsequently pyrolyzes sufficient fuel material to allow combustion with the oxygen liberated by the thermal decomposition of the peroxide. Full ignition latencies after initiation of the peroxide flow are typically less that 1 second. Multiple on-demand relights and higher specific impulse are provided with this system.

A variety of system geometries were investigated, and a best solution using a dual injection system with symmetrical 4-port GOX injector and a single hollow cone injector. GOX pre-leads as short as 0.5 seconds were demonstrated to initiate combustion. At the low mass flux levels desired for this testing campaign, it was demonstrated that a pressure drop of at least 40 psia was required to ensure combustion stability. Using the "best" available configuration as developed by the early tests, a series of evaluation burns were performed with data collected from 10 burns each 90% peroxide and ABS. Results demonstrated mean specific impulse values of *approximately 215 s*. The measured regression rate curves for H_2O_2/ABS generally exhibited reasonable magnitude agreements with data previously collected for ABS and HTPB using gaseous oxygen and nitrous oxide as oxidizers. These comparative agreements support the methodology used to calculate the regression rates. The resulting regression rate curves did, however, demonstrate shape behaviors that were significantly different than those predicted by classical Marxman theory, and as previously measured using nitrous oxide. The predicted peroxide burn exponents are more than 25% lower than the traditional predicted by Marxman for both ABS and HTPB. The lowered burn exponents results in a smaller oxidizer-to-fuel ratio shifts than predicted by conventional theory.

The graphite nozzle used for this test series was slightly over-expanded at the chamber pressure required for stable operation. Thus, the delivered Isp was approximately 2-3% lower than optimal for the test altitude. However, when the results obtained for the ambient test conditions are extrapolated to a hard-vacuum environment, by assuming a 25:1 expansion ratio nozzle, the specific impulse for both fuels grows to greater than *300 s*. This result is very exciting, since a vacuum specific impulse of *300 s* is approximately 30% higher than can be achieved by the current state of the art propellant for in-space propulsion, hydrazine; and greater than 25% higher than can be achieved by the two most promising emerging "green" in-space monopropellants, LMP-103s or AF-M315E. The peroxide/ABS system outperforms the other propellants in every measureable category, including required ignition input energy. When fully developed, a peroxide-based hybrid system could revolutionize the commercial space industry by offering a high-performing, but inherently safe, space propulsion option for rideshare payloads, and other space propulsion applications. *The technology is potentially market disruptive*.

Acknowledgements

This work was funded through NASA STTR Solicitation T1.01, *Affordable Nano/Micro Launch Propulsion Stages* NASA STTR Phase II (T1.01-9931). The Award number is NNX16CD27C and is operated as a Collaborative Agreement (CA) between Utah State University, Logan UT and Parabilis Space Systems, Inc, San Marcos CA.

Conflict of interest

Authors declare that there is no conflict of interest.

References

1. King SM, Marx PC, Taylor D. *The Aerospace Corporation Shell 405 Catalyst Evaluation Program, Volume I: Physical and Catalytic Properties*. USAF Report No. SAMO-TR-271, Los Angeles: Aerodynamics and Propulsion Research Laboratory; 1969. 40 p.
2. Choudhary G, Hansen H, Donkin S, et al. *Toxicological Profile for Hydrazines*. Atlanta, GA: US Department of Health and Human Services Public Health Service Agency for Toxic Substances and Disease Registry (ATSDR); 1997. 224 p.
3. DeSain John D. *Green Propulsion: Trends and Perspectives*; 2012.
4. Goldstein E. The Greening of Satellite Propulsion. *Aerospace America*. 2012;50(2):26–28.
5. Bombelli V. *Economic Benefits for the Use of Non-toxic Monopropellants for Spacecraft Applications*. Huntsville, AL: 39th AIAA/ASME/SAE/ASEE Joint Propulsion Conference and Exhibit; 2003.
6. Haeseler D, Bombelli V, Vuillermoz P, et al. *Green Propellant Propulsion Concepts for Space Transportation and Technology Development Needs*. Cagliari, Sardinia, Italy: Proceedings of the 2nd International Conference on Green Propellants for Space Propulsion; 2004.
7. Venkatachalam S, Santhosh G, Ninan KN. An Overview on the Synthetic Routes and Properties of Ammonium Dinitramide (ADN) and other Dinitramide Salts. *Propellants, Explosives, Pyrotechnics*. 2004;29(3):178–187.
8. Rheingold AL, Cronin JT, Brill TB, et al. Structure of Hydroxylammonium Nitrate (HAN) and the Deuterium Homolog. *Acta Crystallographica*. 1987;43(1):402–404.
9. Hawkins TW, Brand AJ, McKay MB, et al. *Reduced Toxicity, High performance Monopropellant at the U.S. Air Force Research Laboratory*. Huntsville: 4th International Association for the Advancement of Space Safety Conference; 2010. 8 p.
10. Meinhart D. *Selection of Alternate Fuels for HAN-BASED Monopropellants*. 27th JANAFF PDCS and 16th S&EPS Joint Meeting, NTRS; 1998. 143–147 p.
11. Persson M, Anflo K, Dinardi A. *A Family of Thrusters for ADN-Based Monopropellant LMP-103S*. Georgia: 48th AIAA/ASME/SAE/ASEE Joint Propulsion Conference & Exhibit; 2012.
12. *Green Propellant Infusion Mission Propulsion System Development*. San Jose CA: 49th AIAA/ASME/SAE/ASEE Joint Propulsion Conference & Exhibit; 2013.

13. Katsumi T, Hori K. *Combustion Wave Structure of Hydroxylammonium Nitrate Aqueous Solutions*. Nashville: 46th AIAA/ASME/SAE/ASEE Joint Propulsion Conference & Exhibit; 2010.
14. Anon. *Hazard Analysis of Commercial Space Transportation; Vol. 1: Operations, Vol. 2: Hazards, vol. 3: Risk Analysis*. U.S. Dept. of Transportation; 1988.
15. Stephen AW, Nathan RI, Daniel PM, et al. Development of a Power-Efficient, Restart-Capable Arc Ignitor for Hybrid Rockets. *Journal of Propulsion and Power*. 2015;31(6):1739–1749.
16. Whitmore SA, Chamberlain BL. *Consumable Spacecraft Structures with Integrated, 3-D Printed ABS Thrusters*. 53rd AIAA/SAE/ASEE Joint Propulsion Conference; 2017.
17. Whitmore SA. Three-Dimensional Printing of "Green" Fuels for Low-Cost Small Spacecraft Propulsion Systems. *Journal of Spacecraft and Rockets*. 2017;54(6):1–16.
18. Stephen A Whitmore. Advantages of Using Additive manufacturing to Build "Green" Fuels for Hybrid Propulsion. *International Journal of Astronautics an Aeronautical Engineering*. 2017;2(1):1–12.
19. Easton MF, Mitchell AG, Wynne-Jones WFK. The behaviour of mixtures of hydrogen peroxide and water. *Transactions of the Faraday Society*. 1952;48:796–801.
20. Rusek JJ. *Hydrogen Peroxide for Rocket Propulsion Applications*. Phillips Laboratory Report No. PL-TL-96-3015, California: Edwards AFB; 1995.
21. Munday TCF, Darbee L R, McCormick JC. *Investigation of Decomposition Catalysts for 98% Hydrogen Peroxide*. Air Force Rocket Propulsion Laboratory Report No. AFRPL-TR-67-141, California: Edwards Air Force Base; 1967.
22. Runckel JF, Willis CM, Salters LB. *Investigation of Catalyst Beds for 98-Percent-Concentration Hydrogen Peroxide*. Hampton, Virginia: NASA TN D-1808; 1963.
23. Rice FO, Reiff OM. The Thermal Decomposition of Hydrogen Peroxide. *J Phys Chem*. 1927;31(9):1352–1356.
24. Gordon S, McBride BJ. *Computer Program for Calculation of Complex Chemical Equilibrium Compositions and Applications*. NASA RP-1311; 1994. 58 p.
25. Ebelke WH. *Hydrogen Peroxide Handbook*. Air Force Rocket Propulsion Laboratory Report No. AFRPL-TR-67-144, California: Edwards AFB; 1967.
26. Anon. *Thermal Decomposition Measurement of ABS Resin I*. Hitachi Application Brief TA-066e; 1995.
27. Defusco A. *Historical Overview of HTPB The Military's Preferred Solid Propellant Binder for a Half Century*. Defense Systems Information Analysis Center; 2016.
28. Anthoine J, Jean-Yves Lestrade JY, Messineo J, et al. *Performances of a Multi-Pulsed Hybrid Rocket Engine Operating with Highly Concentrated Hydrogen Peroxide*. Georgia: 53rd AIAA/SAE/ASEE Joint Propulsion Conference; 2017.
29. Rommingen JE, Husdal J. *Nammo Hybrid Rocket Propulsion TRL Improvement Program*. 48th AIAA/ASME/SAE/ASEE Joint Propulsion Conference & Exhibit; 2012.
30. Runckel JF, Willis CM Salters LBJ. *Investigation of Catalyst Beds for 98-Percent-Concentration Hydrogen Peroxide*. Hampton, Virginia: National Aeronautics and Space Administration, Langley Station; 1963.
31. Sengupta D, Mazumder S, Cole JV, et al. *Controlling Non-Catalytic Decomposition of High Concentration Hydrogen Peroxide*. AFRL Contract Report # F04611-03-M-3208; 2004.
32. Heister SD, Anderson WE, Corpening JH, et al. *A Model for Thermal decomposition of Hydrogen Peroxide*. AIAA 40th Joint Propulsion Conference, Broward County Convention Center, Fort Lauderdale, Florida; 2004.
33. Mok JS, Helms WJ, Sisco JC, et al. Thermal Decomposition of Hydrogen Peroxide, Part I: Experimental Results. *Journal of Propulsion and Power*. 2005;21(5):942–953.
34. Stephen A Whitmore. Additively Manufactured Acrylonitrile-Butadiene-Styrene–Nitrous-Oxide Hybrid Rocket Motor with Electrostatic Igniter. *J Propulsion and Power*. 2015;31(4):1217–1220.
35. Stephen AW, Stephen LM, Louis T, et al. Survey of Selected Additively Manufactured Propellants for Arc Ignition of Hybrid Rockets. *Journal of Propulsion and Power*. 2016;32(6):1494–1504.
36. Whitmore SA, Peterson ZW, Eilers SD. Comparing Hydroxyl Terminated Polybutadiene and Acrylonitrile Butadiene Styrene as Hybrid Rocket Fuels. *Journal of Propulsion and Power*. 2013;29(3):582–592.
37. Whitmore SA, Mathias S, Harvey R. *High Voltage Breakdown and Arc-Tracking Mechanism of Thermoplastics with Applications to Hybrid Rocket Arc- Ignition*. 53rd AIAA/SAE/ASEE Joint Propulsion Conference, AIAA Propulsion and Energy Forum; 2017.
38. Whitmore SA. Additively Manufactured Acrylonitrile-Butadiene-Styrene–Nitrous-Oxide Hybrid Rocket Motor with Electrostatic Igniter. *Journal of Propulsion and Power*. 2015;31(4):1217–1220.
39. Whitmore SA, Nathan RI, Daniel PM, et al. Development of a Power-Efficient, Restart-Capable Arc Ignitor for Hybrid Rockets. *Journal of Propulsion and Power*. 2015;31(6):1739–1749.
40. Whitmore SA, Merkley DP. *Arc-Ignition of a 70%-85% Hydrogen Peroxide/ABS Hybrid Rocket System*. 53rd AIAA/SAE/ASEE Joint Propulsion Conference, AIAA Propulsion and Energy Forum; 2017.
41. Whitmore SA. Three-Dimensional Printing of "Green" Fuels for Low-Cost Small Spacecraft Propulsion Systems. *Journal of Spacecraft and Rockets*. 2018;55(1):13–26.
42. Whitmore SA, Walker SD, Merkley DP, et al. High Regression Rate Hybrid Rocket Fuel Grains with Helical Port Structures. *Journal of Propulsion and Power*. 2015;31(6):1727–1738.
43. Anthoine J, Jean-Yves Lestrade JY, Messineo J, et al. *Performances of a Multi-Pulsed Hybrid Rocket Engine Operating with Highly Concentrated Hydrogen Peroxide*. 53rd AIAA/SAE/ASEE Joint Propulsion; 2017.
44. Yasensky D, Larson C, Reali J, et al. *Citric Acid passivation of Stainless Steel*. Presentation to the Aircraft Airworthiness and Sustainment Conference; 2011. 175 p.
45. Anon. *Passivation of Corrosion Resistant Steels*. SAE International Standard; 2011.
46. Sutton GP, Biblarz O. *Rocket Propulsion Elements,* 7th ed. New York: Wiley Publishing, Inc; 2001. 197–238 p.
47. Krevelen DV, Chermin H. Estimation of the Free Enthalpy (Gibbs Free Energy) of Formation of Organic Compounds from Group Contributions. *Chemical Engineering Science*. 1951;1(2):66–80.
48. Beckwith TG, Marangoni RD, Lienhard VJH. *Mechanical Measurements*, 6th edn. Prentice Hall; 2006. 43–73 p.
49. Whitmore SA, Walker SD, Merkley DP, et al. High Regression Rate Hybrid Rocket Fuel Grains with Helical Port Structures. *Journal of Propulsion and Power*. 2015;31(6):1727–1738.

50. Whitmore SA, Merkley SL. *Effects of Radiation Heating on Additively Printed Hybrid Fuel Grain O/F Shift*. 52nd AIAA/SAE/ASEE Joint Propulsion Conference, AIAA Propulsion and Energy Forum; 2016.

51. Pastrone D. Approaches to Low Fuel Regression Rate in Hybrid Rocket Motors. *International Journal of Aeronautical Engineering.* 2012;649753:1–12.

52. Marxman G, Gilbert M. Turbulent Boundary Layer Combustion in the Hybrid Rocket. *International Symposium on Combustion.* 1963;9(1):371–383.

53. Marxman GA, Wooldridge CE, Muzzy RJ. Fundamentals of Hybrid Boundary Combustion. *Progress in Astronautics and Aeronautics.* 1964;15(1):485.

54. Brand Adam. *Reduced Toxicity High Performance Monopropellant*. AFRL-RZ-ED-VG-2011-326, Stockholm Sweden: Green Propellants Workshop; 2011.